Non-equilibrium rate theory for polariton relaxation dynamics ⊘

Special Collection: Polaritonics for Next Generation Materials

Yifan Lai (ID) ; Wenxiang Ying (ID) ; Pengfei Huo ✉ (ID)
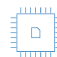
Check for updates

View Online   Export Citation

Non-equilibrium rate theory for polariton relaxation dynamics

View Online   Export Citation   CrossMark

Yifan Lai,[1,a)] [iD] Wenxiang Ying,[1] [iD] and Pengfei Huo[1,2,b)] [iD]

AFFILIATIONS

[1] Department of Chemistry, University of Rochester, 120 Trustee Road, Rochester, New York 14627, USA
[2] The Institute of Optics, Hajim School of Engineering, University of Rochester, Rochester, New York 14627, USA

Note: This paper is part of the JCP Special Topic on Polaritonics for Next Generation Materials.
[a)] Electronic mail: ylai19@ur.rochester.edu
[b)] Author to whom correspondence should be addressed: pengfei.huo@rochester.edu

ABSTRACT

We derive an analytic expression of the non-equilibrium Fermi's golden rule (NE-FGR) expression for a Holstein–Tavis–Cumming Hamiltonian, a universal model for many molecules collectively coupled to the optical cavity. These NE-FGR expressions capture the full-time-dependent behavior of the rate constant for transitions from polariton states to dark states. The rate is shown to be reduced to the well-known frequency domain-based equilibrium Fermi's golden rule (E-FGR) expression in the equilibrium and collective limit and is shown to retain the same scaling with the number of sites in non-equilibrium and non-collective cases. We use these NE-FGR to perform population dynamics with a time-non-local and time-local quantum master equation and obtain accurate population dynamics from the initially occupied upper or lower polariton states. Furthermore, NE-FGR significantly improves the accuracy of the population dynamics when starting from the lower polariton compared to the E-FGR theory, highlighting the importance of the non-Markovian behavior and the short-time transient behavior in the transition rate constant.

Published under an exclusive license by AIP Publishing. https://doi.org/10.1063/5.0231396

I. INTRODUCTION

Coupling molecules inside an optical cavity generates polaritons, which have been the target of interest in recent years. These hybrid polariton states arise from strong coupling between molecular states (electronic or vibrational excitations) and quantized Fock states of a cavity-confined radiation mode inside.[1,2] The formation and subsequent dynamics of the polariton states are hypothesized to be the key to various important phenomena, such as cavity-induced alternation of chemical reactivity[3–17] as well as the enhanced transport of exciton-polaritons.[18–28]

In this work, we investigate the excitonic polariton relaxation process, where the excited states of N molecules (hereon referred to as *sites*) are coupled to the photonic excitation of the cavity. The system consists of two polaritonic states that are highly delocalized mixtures of the photon state and excited states of a large number of sites (for $N \sim 10^6$–10^{12}), as well as a large number of dark states (a total of $N - 1$ of them) with purely excitonic character, and carry zero transition dipole from the ground state (hence optically dark). The coupling, and corresponding population transfer as a result, in between the polaritonic as well as the dark state is facilitated by the

nuclear/phonon (hereon referred to as the *bath*) degrees of freedom (DOF). This is crucial for an accurate description of the polariton relaxation process, as demonstrated by the collective scaling of the transfer rates between the polariton and dark states[29–32] as well as the polaron decoupling effect observed in the collective limit,[33–36] the interesting energy gap law,[37] and phonon and polariton bottleneck effect.[38]

While the relaxation process of cavity polariton has been the subject of various experimental studies,[12,37,39–43] accurate simulation of the population dynamics is essential to the theoretical studies of an excitonic polaritonic system. Numerically exact methods, such as multi-configurational time-dependent Hartree[44–46] (MCTDH) and its multilayer extension,[47,48] and hierarchical equations of motion[49–52] (HEOM), adopt full quantum mechanical treatment of every DOF, often facing the challenge of a rapidly increasing computational cost when increasing the number of molecules N. Reported simulation of collective dynamics using truncated equations[32] (CUT-E) takes advantage of the permutational symmetry of the material states and can significantly reduce the computational cost through an effective $1/N$ expansion. Mixed-quantum-classical (MQC) methods[36,53,54] treat bath DOF classically and are feasible for

16 September 2024 13:37:38

stimulating a large number of molecules N collectively coupled to the cavity. These methods have been applied previously to study the collective behavior of the polaritonic dynamics.[20,55]

Reduced population dynamics based on transfer rates represent an alternative way to investigate the polariton population dynamics.[56,57] These approaches often use the well-known Fermi's golden rule (FGR) to the polariton dynamics[11,14,31,32,58–61] to describe the transition rate and simulate the population dynamics. The population transfer rates between polariton states and dark states can be obtained without any explicit propagation of the bath equation of motion (EOM) and, in principle, can be performed with an arbitrarily large number of sites N. Another strength of the rate-based approach is the decomposition of the EOM into explicit transfer rates, which provides valuable physical intuition to the underlying dynamics.[56] However, the widely known conventional frequency-domain formulation of FGR, commonly referred to as the equilibrium Fermi's golden rule (E-FGR), assumes that the bath DOF initial condition is at equilibrium with the initial system state, which is not necessarily valid upon photoexcitation.[57] Additionally, E-FGR leads to a fully Markovian EOM, which means a different time-dependent rate equation is required to capture any non-Markovian characteristics of the dynamics.

In this work, we follow a quantum master equation (QME)-based time-domain formulation and derive various analytic expressions of a non-equilibrium Fermi's golden rule (NE-FGR)[56,62–64] rate constant that reduces to the well-known FGR under proper limits under the long time and collective coupling limit. The NE-FGR theory was first introduced by Sun and Geva[56,62] and was recently generalized to study electronic transitions between multiple states.[63,64] Using these NE-FGR rate expressions, we can explicitly perform simulations of the population dynamics using a non-Markovian EOM. This formulation also offers an improvement upon the existing QME-based approach in which no explicit discretization of the spectral density is performed, eliminating this source of additional numerical inaccuracy.[65–67] The accuracy and efficacy of the NE-FGR approach are showcased via the population dynamics of a model polaritonic system with relatively weak system–bath coupling by comparing it to the numerically exact HEOM results. We demonstrate that NE-FGR population dynamics are very accurate in this case, and for the case of lower polariton being initially populated, we report significant non-Markovian characteristics in the dynamics, which requires NE-FGR to capture properly.

II. MODEL AND METHODS

A. Holstein–Tavis–Cumming Hamiltonian

We consider a collection of N two-level systems (molecules, referred to as sites) coupled inside a cavity, described by the following Holstein–Tavis–Cummings (HTC) model:[33,34,40,68]

$$\hat{H} = \hbar\omega_x \sum_{n=0}^{N-1} |X_n\rangle\langle X_n| + \hbar\omega_c \hat{a}^\dagger \hat{a} + \hat{H}_b + \hat{H}_{sb}$$
$$+ \hbar g_c \sum_{n=0}^{N-1} \left(\hat{a}^\dagger |G_n\rangle\langle X_n| + \hat{a}|X_n\rangle\langle G_n| \right). \quad (1)$$

Here, $\hbar\omega_x$ is the exciton site energy, $n \in \{0, 1, \ldots, N-1\}$ is the site index, $|G_n\rangle$ and $|X_n\rangle$ are the ground state and the excited state of

site n, respectively, $\hat{a}^\dagger$ and $\hat{a}$ are the creation and annihilation operators of the cavity photons with frequency ω_c, respectively, and g_c is the single molecule light–matter coupling strength. Experimentally, it was estimated that $N = 10^6$–10^{12} molecules are collectively coupled to one cavity mode, which was referred to as the collective coupling limit.[1]

Each site (molecule) is coupled to its independent phonon environment, which is modeled as the bath Hamiltonian $\hat{H}_b + \hat{H}_{sb}$. These baths are assumed to be harmonic and identical for all sites n, expressed as follows:

$$\hat{H}_b = \sum_n \sum_a \hbar\omega_a \hat{b}_{a,n}^\dagger \hat{b}_{a,n}, \quad (2a)$$

$$\hat{H}_{sb} = \sum_n |X_n\rangle\langle X_n| \otimes \sum_a c_a \left(\hat{b}_{a,n}^\dagger + \hat{b}_{a,n} \right), \quad (2b)$$

where a is the bath mode index, and $\hat{b}_{a,n}^\dagger$ are the raising operators for the $a-$th harmonic bath mode of the $n-$th site, with frequency ω_a. The exciton–phonon coupling is characterized by the spectral density defined as[69]

$$J(\omega) = \pi\hbar^{-1} \sum_a c_a^2 \delta(\omega - \omega_a). \quad (3)$$

In the current study, we refer to the electronic and the photonic DOFs as the *system* DOFs, leaving everything else as the *bath* DOFs.

In this work, we derive the non-equilibrium Fermi's golden rule (NE-FGR) theory for the polariton relaxation processes and simulate the polariton relaxation dynamics via quantum master equation approaches. The application of such a perturbative population dynamics method (i.e., the NE-FGR rate theory) implies that the off-diagonal elements of the Hamiltonian are treated as a perturbation. For the system DOF, the polariton basis is used such that the system Hamiltonian is diagonalized. In this case, the exciton–phonon couplings become the perturbation.

We start by transforming the Hamiltonian from the site basis to the delocalized eigenbasis[31] using the collective excitation/de-excitation operators[36,70,71] for the bright state [which is $j = 0$ in Eq. (5)] as

$$\hat{B}^\dagger = \frac{1}{\sqrt{N}} \sum_{n=0}^{N-1} |X_n\rangle\langle G_n|, \quad (4a)$$

$$\hat{B} = \frac{1}{\sqrt{N}} \sum_{n=0}^{N-1} |G_n\rangle\langle X_n| \quad (4b)$$

as well as for the Dark states for $j = 1, 2, \ldots, N-1$ as

$$\hat{D}_j^\dagger = \frac{1}{\sqrt{N}} \sum_{n=0}^{N-1} \exp\left(-2\pi i \frac{nj}{N}\right)|X_n\rangle\langle G_n|, \quad (5a)$$

$$\hat{D}_j = \frac{1}{\sqrt{N}} \sum_{n=0}^{N-1} \exp\left(2\pi i \frac{nj}{N}\right)|G_n\rangle\langle X_n|, \quad (5b)$$

where we adopt first and second quantization notations. Throughout this paper, we only consider the single excitation subspace.

16 September 2024 13:37:38

As one can see from Eq. (5), these dark states are composed of the delocalized exciton states. These bright and dark states are mutually orthogonal, and the dark states are optically dark $\langle G|\hat{\mu}|D_j\rangle = (\mu_{eg}/\sqrt{N}) \cdot \sum_{n=0}^{N-1} \exp(-2\pi i \frac{nj}{N}) = 0$ (we assume that all molecules have identical transition dipoles). In addition, note that the choice of the dark states is not unique and other choices are possible [see Eq. (8) in Ref. 72 for the Schur–Weyl basis].

To differentiate between the site basis and the delocalized basis, $\{m, n, \ldots\}$ will be used to index the site basis, while $\{j, k, \ldots\}$ will be used to index the delocalized basis. Specifically, $j = 0$ corresponds to an all-symmetric entity (i.e., the bright state), while $j = 1, 2, \ldots, N-1$ are asymmetrical (i.e., dark states). Furthermore, the $\{j, k, \ldots\} \in [0, N-1]$ are defined explicitly in the reciprocal space such that $-j \equiv N - j$ and $j - k \equiv N + j - k$ for $j < k$.

The same transformation also applies to the phonon bath DOF, generating a set of delocalized reciprocal-space bath modes $\hat{v}_{a,j}^\dagger$. The asymmetrical ($j = 1, 2, \ldots, N-1$) bath modes are defined as

$$\hat{v}_{a,j}^\dagger = \frac{1}{\sqrt{N}} \sum_{n=0}^{N-1} \exp\left(-2\pi i \frac{nj}{N}\right) \hat{b}_{a,n}^\dagger, \qquad (6a)$$

$$\hat{v}_{a,j} = \frac{1}{\sqrt{N}} \sum_{n=0}^{N-1} \exp\left(2\pi i \frac{nj}{N}\right) \hat{b}_{a,n}, \qquad (6b)$$

while the symmetrical ($j = 0$) phonon bath modes are expressed as

$$\hat{v}_{a,0}^\dagger = \frac{1}{\sqrt{N}} \sum_{n=0}^{N-1} \hat{b}_{a,n}^\dagger. \qquad (6c)$$

Readers may refer to Eq. (A1) in Appendix A for an explicit expression of the Hamiltonian in the reciprocal space.

The *diabatic* polaritonic Hamiltonian (also known as the Tavis–Cummings Hamiltonian[70]) is the system Hamiltonian $\hat{H}_{pl} = \hat{H} - (\hat{H}_b + \hat{H}_{sb})$, whose eigenstates are two bright polariton states and $N-1$ dark states (with zero transition dipole from the overall ground state $|G\rangle \otimes |0\rangle$). In the single exciton basis, the upper polariton state (UP or $|+\rangle$) and lower polariton state (LP or $|-\rangle$) are superpositions of the bright exciton state ($|B\rangle = \hat{B}^\dagger|G\rangle$), expressed as

$$|+\rangle = \sin \phi \, |G\rangle \otimes |1\rangle + \cos \phi \, |B\rangle \otimes |0\rangle, \qquad (7a)$$

$$|-\rangle = \cos \phi \, |G\rangle \otimes |1\rangle - \sin \phi \, |B\rangle \otimes |0\rangle, \qquad (7b)$$

with the mixing angle ϕ expressed as

$$\phi = \frac{1}{2} \tan^{-1}\left(\frac{2\sqrt{N}g_c}{\omega_x - \omega_c}\right) \in \left[0, \frac{\pi}{2}\right) \qquad (8)$$

and the energy of the polaritons expressed as

$$\omega_\pm = \frac{\omega_x + \omega_c}{2} \pm \frac{1}{2}\sqrt{4Ng_c^2 + (\omega_x - \omega_c)^2}. \qquad (9)$$

The corresponding raising operators are expressed as

$$\hat{P}_+^\dagger = \sin \phi \, \hat{a}^\dagger + \cos \phi \, \hat{B}^\dagger, \qquad (10a)$$

$$\hat{P}_-^\dagger = \cos \phi \, \hat{a}^\dagger - \sin \phi \, \hat{B}^\dagger. \qquad (10b)$$

In the polaritonic basis, the Hamiltonian is expressed in Eq. (A2) in Appendix A. We further define the detuning between the photon energy and matter excitation as $\Delta = \omega_c - \omega_x$.

B. Non-equilibrium Fermi's golden rule (NE-FGR)

To investigate the polariton relaxation process, we derive the expression of the non-equilibrium Fermi's golden rule (NE-FGR) theory for the HTC Hamiltonian expressed in Eq. (A2). NE-FGR has been previously developed to investigate photoinduced charge transfer processes by Sun, Geva, and co-workers.[56,57] Note that NE-FGR treats the off-diagonal elements of the Hamiltonian as a small perturbation, which in the polariton basis effectively assumes weak system–bath coupling (exciton–phonon coupling).

This assumption is expected to be valid when N becomes larger since all off-diagonal exciton–phonon coupling terms in Eq. (A2) scales with $1/\sqrt{N}$, reducing the magnitude of the polariton–phonon coupling as N enters the collective limit (for $N = 10^6$–10^{12}). This is indeed the case for the $\hat{P}_+^\dagger \hat{P}_+ \otimes \sum_a \frac{c_a}{\sqrt{N}}(\hat{v}_{a,0}^\dagger + \hat{v}_{a,0})$ term [second line in Eq. (A2)] as well as for the $\hat{P}_-^\dagger \hat{P}_-$ term, where the exciton–phonon coupling for the polariton state and the re-organization energy will decay when N increases, commonly known as the polaron decoupling mechanism. Such straightforward scaling is not applicable to $\sum_{j=1}^{N-1} \hat{P}_+^\dagger \hat{D}_j \otimes \sum_a \frac{c_a}{\sqrt{N}}(\hat{v}_{a,j}^\dagger + \hat{v}_{a,-j})$ due to the $N-1$ multiplicity of the dark states, as demonstrated later in this work [see Eq. (30a), the transition rate from $|\pm\rangle$ to the dark state manifold scales as $(N-1)/N = \mathcal{O}(1)$.] Future work is still required to confirm if increasing N will make perturbative treatment more valid.

Following previous work on time-domain derivation of Fermi's golden rule via the quantum master equation (QME),[56,57,62,73] we begin with the following time-nonlocal (TNL) population equation of motion (EOM):

$$\frac{d}{dt}P_j(t) = -\frac{1}{\hbar^2}\sum_k \int_0^t ds \, \mathcal{K}_{jk}(t,s)P_k(t-s), \qquad (11)$$

which is obtained by defining the population projection superoperator $\mathcal{P}$ in the Nakajima–Zwanzig equation as $\mathcal{P}\hat{O} = \sum_j |j\rangle\langle j|\langle j|\hat{O}|j\rangle$, following a second order perturbative approximation, with details provided in Ref. 56. In Eq. (11), P_j is the time-dependent population for state $|j\rangle \in \{|\pm\rangle, |D_1\rangle, |D_2\rangle, \ldots, |D_{N-1}\rangle\}$, and the population memory kernel $\mathcal{K}_{jk}$ is expressed as

$$\mathcal{K}_{jk}(t,s) = \delta_{kj} \cdot 2\mathrm{Re}\left[\sum_{l \neq j} C_{j \to l}(t,s)\right] - 2\mathrm{Re}\left[C_{k \to j}(t,s)\right], \qquad (12)$$

in which the correlation function $C_{i \to f}$ corresponds to the population transfer process $i \to f$, expressed as

$$C_{i \to f}(t,s) = \mathrm{Tr}_b\left[\hat{\rho}_b(0)e^{\frac{i}{\hbar}\hat{H}_i(t)}\hat{H}_{if}e^{-\frac{i}{\hbar}\hat{H}_f(s)}\hat{H}_{fi}e^{-\frac{i}{\hbar}\hat{H}_i(t-s)}\right]. \qquad (13)$$

Here, $\hat{H}_k = \langle k|\hat{H}|k\rangle$ denotes the diagonal elements of the Hamiltonian in Eq. (A2), while $\hat{H}_{jk} = \langle j|\hat{H}|k\rangle$ denotes the off-diagonal elements, $\{|k\rangle, |j\rangle\} \in \{|\pm\rangle, |D_j\rangle\}$. Note that $\hat{H}_k$ and $\hat{H}_{jk}$ are still operators of the bath DOFs.

To evaluate the correlation function in Eq. (13), we decompose $\hat{H}_k$ and $\hat{H}_{jk}$ terms into single-mode entities (for the ath mode) according to the detailed Hamiltonian expression in Eq. (A2), yielding

$$\hat{H}_k = \hbar\omega_k + \sum_a \sum_{j'=0}^{N-1} \hat{h}_a^{j'} + \sum_a \hat{H}_{a,k}, \quad (14a)$$

$$\hat{h}_a^{j'} = \hbar\omega_a \hat{v}_{a,j'}^\dagger \hat{v}_{a,j'}, \quad (14b)$$

$$\hat{H}_{jk} = \sum_a \hat{H}_{a,jk}, \quad (14c)$$

where $\hat{H}_{a,k}$ and $\hat{H}_{a,jk}$ correspond to the coupling between system and bath DOF, see Eq. (20) for their explicit expressions [more details are provided in supplementary material Eqs. (S13) and (S17)]. The initial state of the bath is assumed to be at thermal equilibrium,

$$\hat{\rho}_b(0) = \bigotimes_{a,j} \frac{1}{\mathcal{Z}_{a,j}} \exp\left(-\beta\hbar\omega_a \hat{v}_{a,j}^\dagger \hat{v}_{a,j}\right), \quad (15)$$

where $\mathcal{Z}_{a,j} \equiv \mathrm{Tr}_b\left[\exp\left(-\beta\hbar\omega_a \hat{v}_{a,j}^\dagger \hat{v}_{a,j}\right)\right]$ is the partition function for the bath DOF, $\beta = 1/(k_BT)$ is the inverse temperature, and k_B is the Boltzmann constant.

As a result of the second-order perturbative QME,[73] the time-local variant of the population QME shares the same memory kernel as TNL, expressed as

$$\frac{d}{dt}P_j(t) = -\frac{1}{\hbar^2}\sum_k \left[\int_0^t ds\, \mathcal{K}_{jk}(t,s)\right]P_k(t). \quad (16a)$$

This time-local population QME can be cast into an equation of motion (EOM) governed by time-dependent rate constants,

$$\frac{d}{dt}P_j(t) = \sum_{i\neq j} k_{i\rightarrow j}(t)P_i(t) - \sum_{f\neq j} k_{j\rightarrow f}(t)P_j(t), \quad (16b)$$

where the time-dependent rate constant $k_{i\rightarrow f}(t)$ is referred to[56,62] as the non-equilibrium FGR (NE-FGR) and is generated by integrating the corresponding time correlation-function $C_{i\rightarrow f}(t,s)$ as follows:

$$k_{i\rightarrow f}(t) = \frac{2}{\hbar^2}\mathrm{Re}\int_0^t ds\, C_{i\rightarrow f}(t,s), \quad (17)$$

and the equilibrium FGR (E-FGR) is the $t \rightarrow \infty$ limit of $k_{i\rightarrow f}(t)$. Related to the rate constant theory,[74–76] $C_{i\rightarrow f}(t,s)$ is the flux–flux correlation function and $k_{i\rightarrow f}(t)$ is the flux–side correlation function.

We note that the Hamiltonian [Eq. (A2)] is invariant under any permutations among the dark states index; hence, all inter-dark state rates are identical to each other. The same argument can be applied to the population transfer rates between the dark and polariton states such that the $N-1$ dark states are equivalent in the population dynamics. In this work, the polariton relaxation process is investigated by initially populating the polariton state (either $|+\rangle$ or $|-\rangle$) and then simulating the population transfer dynamics to the dark

state. As a result, all dark states have zero initial population and will have the same population throughout the dynamics. Therefore, we instead study the population dynamics of the dark states manifold that have the combined population of all dark states,

$$P_\mathcal{D} = \sum_{j=1}^{N-1} P_j = (N-1)P_j, \quad (18)$$

and define the dark state manifold as

$$|\mathcal{D}\rangle\langle\mathcal{D}| \equiv \sum_j |D_j\rangle\langle D_j|. \quad (19)$$

1. Transition rate between dark states

To evaluate the population transfer correlation functions, we start by looking at the population transfer rate between two dark states, $j \neq \pm$, and $k \neq \pm$ and $\hbar\omega_j = \hbar\omega_x$ (dark state energy is identical to the exciton energy). The relevant single-mode bath Hamiltonian $\hat{H}_{a,j}$ for the ath mode [defined in Eq. (14)] is expressed as

$$\hat{H}_{a,j} = \frac{c_a}{\sqrt{N}}\left(\hat{v}_{a,0}^\dagger + \hat{v}_{a,0}\right), \quad (20a)$$

which is the diagonal system–bath coupling term that couples one dark state to the fully symmetric bath mode $\hat{v}_{a,0}^\dagger$ [the $\sum_{j=1}^{N-1}\hat{D}_j^\dagger\hat{D}_j^\dagger$ term in Eq. (A2)]. Since all dark states are shifted by the symmetric bath mode with exactly the same magnitude, this term does not contribute to the dark-to-dark correlation function. Furthermore, the $\hat{H}_{a,jk}$ term defined in Eq. (14) is expressed as

$$\hat{H}_{a,jk} = \frac{c_a}{\sqrt{N}}\left(\hat{v}_{a,k-j}^\dagger + \hat{v}_{a,j-k}\right), \quad (20b)$$

which corresponds to the off-diagonal system–bath coupling [the $\sum_{j\neq k}^{N-1}\hat{D}_j^\dagger\hat{D}_k$ term in Eq. (A2)]. This term causes the transition from $|D_k\rangle$ to $|D_j\rangle$ through the annihilation (creation) of phonons with the reciprocal index matching (complementary to) the transition.

Since $\hat{H}_{a,jk}$ is the only term that contributes to the population transfer between dark states, such transitions are equivalent to a population transfer between *unshifted* harmonic oscillators, *only* involving contributions from off-diagonal system–bath coupling. The correlation function is given by (for details of the derivation, see Sec. II A of the supplementary material)

$$C_{j\rightarrow k}(t,s) \equiv C_{D\rightarrow D}(s)$$
$$= \frac{1}{N}\frac{\hbar}{\pi}\int_0^\infty d\omega\, J(\omega)\left[\coth\left(\frac{1}{2}\beta\hbar\omega\right)\cos\omega s + i\sin\omega s\right]$$
$$\equiv \frac{2}{N\beta}\gamma_\beta(s) + \frac{i\hbar}{N}\dot{\gamma}(s), \quad (21)$$

where $J(\omega)$ is the spectral density defined in Eq. (3). In the above expression [Eq. (21)], we denote all of the $C_{j\rightarrow k}(t,s)$ as $C_{D\rightarrow D}(s)$ because they are all identical. The single-site friction kernel[77] $\gamma(s)$, $\dot{\gamma}(s)$ as well as the finite-temperature friction kernel $\gamma_\beta(s)$ are expressed as

$$\gamma_\beta(s) = \frac{\beta\hbar}{2\pi}\int_0^\infty d\omega\, J(\omega)\cdot\coth\left(\frac{1}{2}\beta\hbar\omega\right)\cos(\omega s), \quad (22a)$$

$$\gamma(s) = \gamma_{\beta=0}(s) = \frac{1}{\pi} \int_0^\infty d\omega \, \frac{J(\omega)}{\omega} \cos(\omega s), \qquad (22b)$$

$$\dot{\gamma}(s) = \frac{1}{\pi} \int_0^\infty d\omega \, J(\omega) \cdot \sin(\omega s). \qquad (22c)$$

This formulation is chosen because $\gamma(s)$ and $\dot{\gamma}(s)$ can be evaluated analytically and $\gamma_\beta(s)$ by numerical integration, as described in more detail in Appendix B.

2. Transition rate between dark states and polaritons

The population transfer correlation functions between the polaritons ($\pm$) and the dark state manifold ($\mathcal{D}$) can be evaluated via a similar procedure, as detailed in Sec. II B of the supplementary material. The final results are

$$C_{\pm\to\mathcal{D}}(t,s) = e^{i(\omega_\pm - \omega_x)s} \cdot (N-1) \cdot C^0_{\pm\to D}(t,s)$$
$$\times \frac{1}{2}(1 \pm \cos 2\phi) \cdot C_{D\to D}(s), \qquad (23a)$$

$$C_{\mathcal{D}\to\pm}(t,s) = e^{-i(\omega_\pm - \omega_x)s} \cdot C^0_{D\to\pm}(t,s)$$
$$\times \frac{1}{2}(1 \pm \cos 2\phi) \cdot C_{D\to D}(s). \qquad (23b)$$

Barring pre-factors and the oscillatory term $e^{\pm i(\omega_\pm - \omega_x)s}$, Eq. (23) contains two major contributions, $C_{D\to D}(s)$ and $C^0_{\mathcal{J}\to\mathcal{K}}(t,s)$ terms. The term $C_{D\to D}(s)$ is the contribution of $\hat{v}_j$ and $\hat{v}_{-j}$ term that provides off-diagonal coupling between the polaritons and a dark state [through the last line in Eq. (A2)]. This $C_{D\to D}(s)$ expression is identical to the case of the dark-to-dark state transition expressed in Eq. (21) since the jth and $-j$th modes are unshifted in the polariton or dark states, as discussed above with the derivation of Eq. (21).

The $C^0_{\mathcal{J}\to\mathcal{K}}(t,s)$ term (for $\{|\mathcal{J},\mathcal{K}\rangle \in \{|\pm\rangle, |\mathcal{D}\rangle\}\}$) in Eq. (23) corresponds to the contribution from symmetric bath modes ($\hat{v}^\dagger_{a,0}$ and $\hat{v}_{a,0}$) in the form of diagonal coupling [see the second line of Eq. (A2)], shifting by different amounts between the polariton states and the dark states [see the second line of Eq. (A2)]. Here, we use C^0 to denote that this contribution originates from the symmetrical phonon $\hat{v}^\dagger_{a,0}$ and $\hat{v}_{a,0}$ coupling to the polariton and dark states. It is evaluated via the Gaussian integral technique[56,57] (for example, Appendix B in Ref. 57) with the details of derivation provided in Sec. II B of the supplementary material. The final expression of $C^0_{\mathcal{J}\to\mathcal{K}}(t,s)$ is

$$C^0_{\mathcal{J}\to\mathcal{K}}(t,s) = \exp \frac{1}{N\hbar} \left\{ -\frac{1}{\beta\hbar}(r_\mathcal{J} - r_\mathcal{K})^2 \bar{\Gamma}_\beta(s) \right.$$
$$+ 2i(r_\mathcal{J} - r_\mathcal{K})r_\mathcal{J}(\Gamma(t) - \Gamma(t-s))$$
$$\left. - i(r_\mathcal{J} - r_\mathcal{K})^2 \Gamma(s) - i(r_\mathcal{J}^2 - r_\mathcal{K}^2)\lambda \cdot s \right\}, \qquad (24)$$

where $\lambda = \gamma(0)$, $r_\mathcal{D} = 1$ and $r_\pm = (1 \pm \cos 2\phi)/2$, $\Gamma_\beta, \bar{\Gamma}_\beta$ are the first and second order antiderivative of γ_β [see Eq. (22a)] expressed as

$$\Gamma_\beta(s) = \int_0^s d\tau \, \gamma_\beta(\tau), \qquad (25a)$$

$$\bar{\Gamma}_\beta(s) = 2 \int_0^s d\tau \, \Gamma_\beta(\tau), \qquad (25b)$$

respectively, with their detailed expressions provided in Eq. (S28) in the supplementary material, and $\Gamma, \bar{\Gamma}$ defined as the high-temperature limit $\beta = 0$ of $\Gamma_\beta(s)$ and $\bar{\Gamma}_\beta(s)$, respectively. Note that $C^0_{\mathcal{J}\to\mathcal{K}}(t,s)$ in Eq. (24) is caused by the difference in phonon mode shift in the dark state (which is fully excitonic) and the polariton states (which have mixed exciton and photon character). The $C^0_{\mathcal{J}\to\mathcal{K}}(t,s)$ term can be interpreted as the non-equilibrium single-site population transfer FGR correlation function[56,57] under the Condon approximation (which is equivalent to setting $\langle \mathcal{J}|\hat{H}_{sb}|\mathcal{K}\rangle = \hat{\mathcal{I}}_b$, the identity operator of the bath DOF). A similar expression is also encountered in the previous work on non-equilibrium FGR by Sun and Geva.[62]

In Eq. (23), the forward rate ($|\pm\rangle \to \{|\mathcal{D}\rangle\}$) and reverse rate ($\{|\mathcal{D}\rangle\} \to |\pm\rangle$) scale differently with the number of sites N. One can clearly see that the transition rate from the $|\pm\rangle$ polariton state to the dark states manifold contains an additional factor $N-1$. This is because there are $N-1$ degenerate dark states as the final state, or equivalently, $N-1$ identical. The reverse transition, $|\mathcal{D}\rangle \to |\pm\rangle$, also consists of $N-1$ identical processes, but each transition is from a single dark state, which has $\propto 1/(N-1)$ of the overall population of the dark state manifold $\{|\mathcal{D}\rangle\}$, leading to no overall scaling with the number of sites ($\propto \mathcal{O}(N^0)$). Taking the $1/N$ scaling of $C_{D\to D}$ into consideration [see Eq. (21)], the dark-to-polariton NE-FGR rate scales with $1/N$, while the polariton-to-dark NE-FGR rate scales with $(N-1)/N$. This scaling in terms of N is consistent with well-known equilibrium FGR polaritonic relaxation rates[31,32] or Lindblad master equations[29,30] and can be confirmed through the recent Mixed Quantum–Classical (MQC) simulations[55] and exact quantum dynamics simulations.[71]

3. Transition rate between polariton states

Finally, the transitions among two polariton states (for $|+\rangle \to |-\rangle$ and $|-\rangle \to |+\rangle$) consist of a minor part of the polariton relaxation process [negligible when N is large, typically for $N > 10$ in the current study as can be seen from panel (f) in Figs. 2–4]. This is because $k_{+\to D} \propto \mathcal{O}(N^0)$ (for a large N limit) and $k_{\pm\to\mp} \propto \mathcal{O}(1/N)$ [see Eq. (30a)]. The inter-polariton transfer is often ignored in the study of polariton lifetime because the dark states usually outnumber the polariton states in the collective coupling regime, and one may reasonably assume that the inter-polariton transition rate is much lower compared to the polariton-dark transition rate. For the sake of completeness, we include the inter-polariton transfer explicitly in the current study such that its effect can be quantified when N is not very large.

In the population transfer correlation function $C_{\pm\to\mp}(t,s)$ from one polariton state to the other, the symmetric bath mode $k = 0$ contributes to both diagonal and off-diagonal coupling. As a result, it is no longer possible to separate the two contributions cleanly like the previously discussed cases, leading to a slightly more complex evaluation via the Gaussian integral approach. The details are provided in Sec. II C of the supplementary material. The final result of $C_{\pm\to\mp}(t,s)$ is expressed as

$$C_{\pm\to\mp}(t,s) = e^{i(\omega_\pm - \omega_\mp)s} \cdot \frac{1}{4}\sin^2 2\phi \, C^0_{\pm\to\mp}(t,s)$$
$$\times [F_{\pm\to\mp}(t,s)F_{\pm\to\mp}(t-s,s) + C_{D\to D}(s)], \qquad (26a)$$

where $C_{D\to D}$ is expressed in Eq. (21), $C_{\pm\to\mp}^0(t,s)$ is expressed in Eq. (24), and the auxiliary factors $F_{\pm\to\mp}$ correspond to the non-Condon nature of $C_{\pm\to\mp}(t,s)$ with the following expression:

$$F_{\pm\to\mp}(t,s) = \frac{1}{N}\left[-\lambda \mp \cos 2\phi \cdot \gamma(s) + (1\pm\cos 2\phi)\gamma(t) \right.$$
$$\left. \pm \frac{2i}{\beta\hbar}\cos 2\phi \cdot \Gamma_\beta(s) \right], \qquad (26b)$$

where $\lambda = \gamma(0)$, $\gamma(s)$ is expressed in Eq. (22b), and Γ_β is expressed in Eq. (25).

To summarize, we derived the NE-FGR expressions for polariton transitions as follows:

$$k_{i\to f}(t) = \frac{2}{\hbar^2}\mathrm{Re}\int_0^t ds\, C_{i\to f}(t,s),$$

with $C_{\pm\to D}(t,s)$ and $C_{D\to\pm}(t,s)$ expressed in Eq. (23) and $C_{\pm\to\mp}(t,s)$ expressed in Eq. (26a). In Secs. II C and II D, we further simplify these correlation functions and arrive at approximate FGR rate expressions. This is the first key result of this paper.

C. FGR under the Markovian and the collective limit

The aforementioned NE-FGR [Eq. (17)] can be further simplified via various additional approximations. Most obviously, the rate defined in Eq. (17) is time-dependent, meaning the resulting EOM is not Markovian. To arrive at the more widely used Markovian version of the rate equation, we consider the $t\to\infty$ limit of Eq. (17), and the E-FGR rate constant is expressed as

$$k_{i\to f}(t\to\infty) = -\frac{2}{\hbar^2}\mathrm{Re}\int_0^\infty ds\, C_{i\to f}(\infty,s), \qquad (27)$$

where $C_{i\to f}(\infty,s)$ is expressed as [cf. Eq. (13)]

$$C_{i\to f}(\infty,s) = \mathrm{Tr}_b\left[\hat{\rho}_b(0)e^{\frac{i}{\hbar}\hat{H}_i(s)}\hat{H}_{if}e^{-\frac{i}{\hbar}\hat{H}_f(s)}\hat{H}_{fi}\right],$$

and the Markovian limit of NE-FGR is to assume that $k_{i\to f}(t) = k_{i\to f}(t\to\infty) = k_{i\to f}$. This is achieved by making two approximations,

1. The FGR correlation function $C_{i\to f}(t,s)$ has a short lifetime (in terms of s) compared to the resulting dynamics such that the integral limit can be extended to infinity.

2. The t-dependence in $C_{i\to f}(t,s)$ is also eliminated. This is equivalent to setting $\hat{\rho}_b(0) = \exp(-\beta\hat{H}_i)$ in Eq. (13), meaning the bath is at equilibrium in the initial system state i at $t = 0$, which is why the Markovian FGR is referred to *equilibrium* FGR (E-FGR) in this context.

Another useful limit to consider involves the number of sites N. In the case of molecular sites interacting with a cavity, N is usually in the order of 10^6; for more strongly coupled systems, such as nanoparticles or nanoplatelets,[40] N would be in the order of 10^3. These cases correspond to the limit of $N\to\infty$, hereon referred to as the *collective limit*. More specifically, this refers to the limit where the light–matter coupling has a predominantly collective nature, i.e., the individual coupling g_c is weak such that the Rabi splitting $\Omega_R = 2\sqrt{N}g_c$ is large due to the large N.

Noting that N is large under the collective coupling regime and $1/N$ often appears in the correlation function, one can truncate the correlation functions expressed in Eqs. (23) and (26a) to the lowest non-vanishing order of $1/N$, leading to the following approximations:

(a) Relevant for all correlation functions, $C_{J\to K}^0 = \exp\frac{1}{N\hbar}f(t,s) \to 1$;

(b) For polariton–polariton transfer in Eq. (26a), the $F\times F$ term is dropped since it scales as $1/N^2$ compared to the $C_{D\to D}$ term, which scales $1/N$.

The above approximation leads to the following simplified collective-limit correlation function expression:

$$C_{\pm\to D}(s) = e^{i(\omega_\pm-\omega_x)s}\cdot\frac{N-1}{2}(1\pm\cos 2\phi)\cdot C_{D\to D}(s), \qquad (28a)$$

$$C_{D\to\pm}(s) = e^{-i(\omega_\pm-\omega_x)s}\cdot\frac{1}{2}(1\pm\cos 2\phi)\cdot C_{D\to D}(s), \qquad (28b)$$

$$C_{\pm\to\mp}(s) = e^{i(\omega_\pm-\omega_\mp)s}\cdot\frac{1}{4}\sin^2 2\phi\cdot C_{D\to D}(s), \qquad (28c)$$

and all explicit t-dependence in these correlation functions are dropped due to the fact that under the collective limit, $C_{J\to K}^0\to 1$. Importantly, Eq. (28) is equivalent to the expression of Eq. (21), except for a pre-factor and the oscillatory term. This means that in the collective coupling limit, all transitions can be modeled as population transfer between undisplaced harmonic oscillators just like the dark–dark transition Eq. (21), as pointed out in previous studies of collective effects in cavities.[33,35]

Furthermore, if we substitute Eq. (28a) into Eq. (17) and integrate over ds, we have

$$k_{\pm\to D}(t) = \frac{N-1}{2N\pi\hbar}(1\pm\cos 2\phi)\int_0^\infty d\omega J(\omega)\coth\left(\frac{1}{2}\beta\hbar\omega\right)$$
$$\times\left(\frac{\sin[(\omega+\omega_\pm-\omega_x)t]}{\omega+\omega_\pm-\omega_x} + \frac{\sin[(\omega-\omega_\pm+\omega_x)t]}{\omega-\omega_\pm+\omega_x}\right)$$
$$+ \frac{N-1}{2N\pi\hbar}(1\pm\cos 2\phi)\int_0^\infty d\omega J(\omega)$$
$$\times\left(\frac{\sin[(\omega+\omega_\pm-\omega_x)t]}{\omega+\omega_\pm-\omega_x} - \frac{\sin[(\omega-\omega_\pm+\omega_x)t]}{\omega-\omega_\pm+\omega_x}\right). \qquad (29)$$

Note that, in general, Eq. (29) will not have a closed-analytic expression [for an arbitrary $J(\omega)$ expression]. Nevertheless, Eq. (29) suggests that the NE-FGR rate constant will oscillate and decay in time, as later shown in Figs. 2–4. Equation (29) is the second key result of this work.

Combining the equilibrium approximation $t\to\infty$ and the collective limit ($N\to\infty$ and thus $C_{J\to K}^0\to 1$), the collective equilibrium FGR (E-FGR) rate constants can be obtained analytically. These E-FGR expressions can either be obtained from applying the two above-mentioned approximations or directly taking the $t\to\infty$ limit of Eq. (29) [note that when $1/t\to 0$ the last line in Eq. (29) becomes

the delta function], with the details provided in Appendix C. The final expressions for these well-known E-FGR rate constants are

$$k_{\pm \to \mathcal{D}}(t \to \infty) = \frac{N-1}{N\hbar}(1 \pm \cos 2\phi)\frac{J(|\omega_\pm - \omega_x|)}{|1 - e^{-\beta\hbar(\omega_\pm - \omega_x)}|}, \quad (30a)$$

$$k_{\mathcal{D} \to \pm}(t \to \infty) = \frac{1}{N\hbar}(1 \pm \cos 2\phi)\frac{J(|\omega_x - \omega_\pm|)}{|1 - e^{-\beta\hbar(\omega_x - \omega_\pm)}|}, \quad (30b)$$

$$k_{\pm \to \mp}(t \to \infty) = \frac{1}{2N\hbar}\sin^2 2\phi \frac{J(|\omega_\pm - \omega_\mp|)}{|1 - e^{-\beta\hbar(\omega_\pm - \omega_\mp)}|}. \quad (30c)$$

The above expressions for E-FGR can also be directly obtained from the standard frequency-domain FGR derivation (see details in Sec. III of the supplementary material). The essential scaling of these rates with respect to N remains the same as in the NE-FGR expression, and the same scaling relations are also discovered using Lindblad Equations[29,58,60] and recently through the $1/N$ expansion approach.[32]

The pre-factor $N - 1$ (degeneracy of the dark states manifold) can be interpreted either as the density of state for the dark states or as the effective entropy of the dark states manifold.[78] To demonstrate that, consider the E-FGR rate $|-\rangle \leftrightarrow \{|\mathcal{D}_j\rangle\}$ under the resonance condition $\omega_x - \omega_- = \sqrt{N}g_c$,

$$k_{-\to\mathcal{D}}^{cE} = \frac{1}{2N\hbar} \cdot J(\sqrt{N}g_c)[n(\sqrt{N}g_c) + 1]$$
$$\times \exp\left(-\beta\left[\hbar\sqrt{N}g_c - k_B T \ln(N-1)\right]\right), \quad (31a)$$

$$k_{\mathcal{D}\to-}^{cE} = \frac{1}{2N\hbar} \cdot J(\sqrt{N}g_c)[n(\sqrt{N}g_c) + 1], \quad (31b)$$

where $n(\omega) = 1/[e^{\beta\hbar\omega} - 1]$ is the Bose–Einstein distribution function, and we have combined the pre-factor of $N - 1 = \exp[-\beta k_B T \ln(N-1)]$ into the expression of $k_{-\to\mathcal{D}}^{cE}$. As such, the detailed balance ratio between the two states is $\exp(-\beta[\hbar\sqrt{N}g_c - T \cdot k_B \ln(N-1)])$. Hence, the dark state manifold can also be interpreted as one effective state with the free energy relative to $|-\rangle$ as

$$\Delta G = \hbar\sqrt{N}g_c - k_B T \ln(N-1) \equiv \Delta E - T\Delta S. \quad (31c)$$

Hence, the density of state for the dark state manifold $\ln(N-1)$ is equivalent to an entropy term. This expression of entropy coincides with the existing thermodynamics-based analysis,[78] where the addition of the entropy ΔS to the dark states renders it to be more favorable than the lower polariton when N is sufficiently large.

D. Static disorders in the site energy and dipole orientation

In the current study, we have not considered the static disorder in exciton energy[79–81] or dipole orientation disorder.[82] These static disorders are highly relevant to the realistic experimental condition of molecular systems coupled to the cavity and have been theoretically investigated in the recent literature.[81,82] In particular, a static

exciton energy disorder will add the following diagonal constant terms to the adiabatic Hamiltonian equation (1),

$$\hat{H}_\epsilon = \sum_{n=0}^{N-1} \epsilon_n |X_n\rangle\langle X_n|, \quad (32)$$

where ϵ_n typically satisfies a Gaussian distribution (for inhomogeneous broadening) centered around 0 with a certain width σ. The presence of these terms will nullify the symmetry of the HTC Hamiltonian. Nevertheless, for energy static disorder, one can still apply the same unitary transformation from site basis to reciprocal space polariton basis (which has symmetry) to $\hat{H}_\epsilon$ and $\hat{H}_\theta$, resulting in additional static coupling terms in the polariton basis. For example, $\hat{H}_\epsilon$ in the polariton basis is expressed as

$$\hat{H}_\epsilon = \sum_{j=1}^{N-1} (\cos\phi|D_j\rangle\langle+| - \sin\phi|D_j\rangle\langle-|)\tilde{\epsilon}_j + h.c. + \sum_{j\neq k}|D_j\rangle\langle D_k|\tilde{\epsilon}_{j-k}, \quad (33a)$$

$$\tilde{\epsilon}_{j-k} = \frac{1}{N}\sum_{n=0}^{N-1}\exp\left(2\pi i\frac{n(j-k)}{N}\right)\epsilon_n. \quad (33b)$$

If these static couplings $\tilde{\epsilon}$ are small (in the sense of $\tilde{\epsilon} \ll k_B T$) and can be treated perturbatively, then one can treat them in the same FGR framework, resulting in additional terms in the FGR rate constant; otherwise, they have to be treated non-perturbatively. The potential challenge of including these static couplings among polariton states and dark states is that one can no longer easily group the dark state manifold as we outlined in the current work, and one likely needs additional theoretical effort to incorporate the specific rate constant $k_{\pm \to D_k}$. An alternative strategy to model the static exciton energy disorder is grouping a certain number of degenerated exciton states with the same energy $\hbar\omega_x + \epsilon$ into one bin[83] and including different bins to model static disorder.

On the other hand, an orientational disorder of the dipole operator will add the following off-diagonal term to $\hat{H}$ [Eq. (1)]:

$$\hat{H}_\theta = \hbar g_c \sum_{n=0}^{N-1}(\cos\theta_n - 1)\,\hat{a}^\dagger|G_n\rangle\langle X_n| + h.c., \quad (34)$$

where θ_n is the angle between the transition dipole vector for molecule n and the cavity field polarization direction and is assumed to have an isotropic disorder.[82] In fact, $\hat{H} + \hat{H}_\theta - (\hat{H}_b + \hat{H}_{sb})$ is still directly diagonalizable[84] (due to the generated $\hbar\omega_x$). In the case of zero detuning ($\omega_x - \omega_c = 0$), the polaritons states are

$$|\pm\rangle = \frac{1}{\sqrt{2}}|G\rangle \otimes |1\rangle \pm \sum_{n=1}^{N}\frac{\cos\theta_n}{\chi}|X_n\rangle \otimes |1\rangle, \quad (35)$$

where $\chi = \sqrt{\sum_{m=1}^{N}\cos^2\theta_m}$. The FGR rate constant needs to be derived in these new polariton states and dark states. Future work will explore the effect of incorporating these static energy disorders and the dipole orientational disorders.

III. COMPUTATIONAL DETAILS

To demonstrate the NE-FGR method and compute rate constant and population dynamics, we study the polaritonic dynamics for an HTC model [Eq. (1)] where each site is coupled to its own independent phonon bath, described by an identical spectral density. Here, we use the Brownian oscillator form of the spectral density,

$$J(\omega) = \frac{4\lambda\eta\omega\Omega^2}{(\omega^2 - \Omega^2)^2 + 4\eta^2\omega^2}, \quad (36)$$

where λ is the reorganization energy, Ω is the characteristic frequency of the phonon modes, and η is the coupling strength between the exciton and phonon. The parameters used in the model are given in Table I. These are typical parameters for the recently explored CdSe nanoplatelet coupled to a cavity.[40,85] To explore the effect of a few molecules ($N = 5$) and more realistic collective coupling condition ($N = 10^6$), the half Rabi splitting $\sqrt{N}\hbar g_c$ is kept invariant as the number of sites N changes, which is equivalent to scaling g_c with $\sqrt{N}$.

Figure 1 presets the schematic for the model system considered in this work, with an energy diagram of the relevant states as well as the $J(\omega)/(1 - e^{-\beta\hbar\omega})$ function. Here, we consider three cases for the light–matter detuning, a zero detuning $\Delta = 0$ case where the cavity mode is set to be resonant with the bare site excitation, a positive detuning $\Delta = 142$ meV chosen such that the transition energy between dark states $\mathcal{D}$ and UP is in close resonance with the maximum of $J(\omega)/(1 - e^{-\beta\hbar\omega})$, such that the transition rates involving UP is maximized and a negative detuning $\Delta = -142$ meV where transition rates involving LP is maximized.

For the NE-FGR approach, the population dynamics are computed by solving the EOM for a three-element array $\mathbf{P} = [P_+, P_-, P_{\mathcal{D}}]$, where P_+ (P_-) is the upper (lower) polariton population and $P_{\mathcal{D}}$ is the sum of the $N - 1$ identical dark mode populations. The time local (TL) EOM in Eq. (16a) [which only depends on $P_j(t)$] is solved numerically using the memory kernel in Eq. (12) computed from the correlation function $C_{i \to f}(t, s)$, with expressions in Eqs. (23) and (26a). The EOM is numerically solved using a fourth-order Runge–Kutta algorithm on a quadrature, following the same procedure in Ref. 56. The step size dt for integration is taken to be $dt = 0.1$ fs. Note that solving TL-QME in Eq. (16a) with memory kernel [Eq. (12)] is equivalent to solving the rate equation in Eq. (16b) with the NE-FGR rate [Eq. (17)]. For $N = 10^6$ under the collective coupling limit, numerically, $C_{\pm \to D}^0 = C_{D \to \pm}^0 \to 1$ and $F_{\pm \to \mp}(t, s) \propto \mathcal{O}(N^{-2}) \to 0$, it is safe to ignore them in the calculation. A similar numerical procedure is used to solve the TNL-QME in Eq. (11) [note that it depends on $P_j(t - s)$] with the same memory kernel in Eq. (12).

TABLE I. Model parameters for the present study.

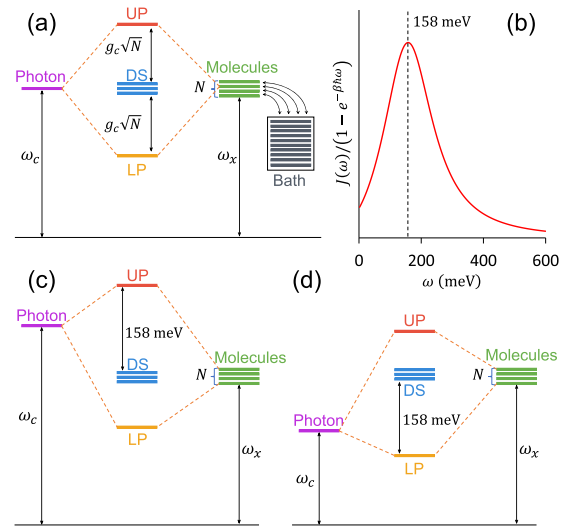| T	λ	$\hbar\Omega$	η	$\hbar\omega_x$	$\sqrt{N}\hbar g_c$
300 K	14 meV	185 meV	0.1 eV	2.0 eV	50 meV

FIG. 1. Schematic Illustration of the model system. (a) The energy diagram of the relevant states in the case of zero detuning, $\Delta = \omega_c - \omega_x = 0$. The site (molecular) states are, in turn, coupled to a set of bath modes. (b) The bath function $J(\omega)/(1 - e^{-\beta\hbar\omega})$ peaks at $\omega = 158$ meV for the chosen model parameter. This is the optimal transition frequency at which the bath promotes a population transfer process in the largest magnitude based on the E-FGR expression [Eq. (30a)]. (c) The energy diagram for the case of positive detuning $\Delta = 142$ meV. The amount of detuning is chosen such that the UP $\to \mathcal{D}$ transition energy exactly matches the optimal frequency of 158 meV. (d) The energy diagram for the case of negative detuning $\Delta = -142$ meV. The amount of detuning is chosen such that the $\mathcal{D} \to$ LP transition matches the optimal frequency of 158 meV.

For the case of E-FGR, the EOM is a simple rate equation [cf. the NE-FGR EOM in Eq. (16b)],

$$\frac{d}{dt}P_j(t) = \sum_{i \neq j} k_{i \to j}(t \to \infty)P_i(t) - \sum_{f \neq j} k_{j \to f}(t \to \infty)P_j(t), \quad (37)$$

where the E-FGR rate $k_{i \to j}(t \to \infty)$ is used as opposed to the NE-FGR rate in the TL EOM in Eq. (16b). The solution of the EOM in Eq. (37) are obtained through the time-evolution matrix $\mathbf{P}(t) = \mathbf{P}(0) \exp(\mathbf{K}t)$, where K is given by

$$\mathbf{K}_{j \neq k} = k_{k \to j}(t \to \infty), \quad \mathbf{K}_{jj} = -\sum_{k \neq j} k_{j \to k}(t \to \infty), \quad (38)$$

where the detailed expressions for these E-FGR rates are provided in Eq. (30a). Note that K is diagonalized to become $\mathbf{K}_{\text{diag}}$ and $\mathbf{K} = \mathbf{U}^{-1}\mathbf{K}_{\text{diag}}\mathbf{U}$, which allows for a straightforward evaluation of population dynamics,

$$\mathbf{P}(t) = \mathbf{P}(0)\mathbf{U}^{-1}\exp(t\mathbf{K}_{\text{diag}})\mathbf{U}. \quad (39)$$

For $N = 5$, we have simulated the quantum dynamics using the numerically exact Hierarchical Equations of Motion (HEOM) approach using the Padé spectral decomposition (PSD),[86–88] with details provided in Sec. IV of the supplementary material.

IV. RESULTS AND DISCUSSIONS

Figure 2 shows the population transfer rates between the two polaritons and the dark states in the zero detuning case $\omega_x = \omega_c$, with $N = 5$ (dashed lines) and $N = 10^6$ (solid lines). The Rabi splitting $2\sqrt{N}g_c$ is kept invariant. Consistent with previous works on NE-FGR,[62] the time-dependent rates converge to the corresponding E-FGR rate after a transient period of time, in this case, ~50 fs.

Panel (f) of Fig. 2 shows the E-FGR rates responsible for the dynamics beyond the transient non-equilibrium period, as a function of N. Four E-FGR rates, $k_{D \rightarrow \pm}$ and $k_{\pm \rightarrow \mp}$, decreases as N increases. On the log–log scale, these four E-FGR rates form straight lines with a slope of -1, meaning these rates scale with $1/N$. Such scaling comes naturally in the collective limit [$N = 10^3$ and $N = 10^6$, Eq. (30a)] but not in the non-collective case [$N = 5$ and $N = 50$, Fourier transform of Eqs. (23) and (26a)] due to the $C^0(t, s)$ term. The fact that the
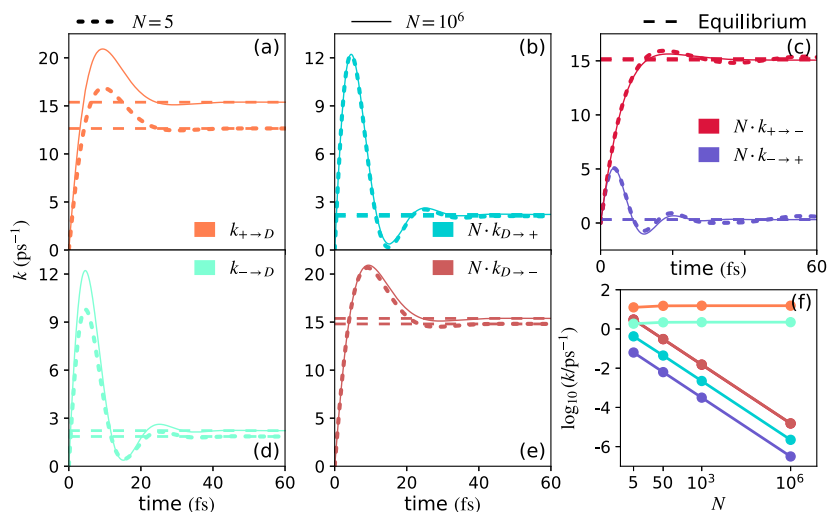

FIG. 2. The E-FGR and NE-FGR population transfer rates between the relevant states for the zero detuning case $\Delta = 0$ meV, for (a) $|+\rangle \rightarrow |\mathcal{D}\rangle$, (b) $|\mathcal{D}\rangle \rightarrow |+\rangle$, (c) $|\pm\rangle \rightarrow |\mp\rangle$, (d) $|-\rangle \rightarrow |\mathcal{D}\rangle$, and (e) $|\mathcal{D}\rangle \rightarrow |-\rangle$. The short dashed horizontal lines correspond to the time-independent E-FGR rates. For NE-FGR, rates for $N = 5$ (short dashed line) and $N = 10^6$ (thin solid line) are presented, where the former is calculated using Eqs. (23), (26a), and (27), and the latter within collective approximation is calculated using Eqs. (28) and (30a). To better showcase rates at different N values in the same order of magnitude, the dark-to-polariton and polariton–polariton rates are scaled by a factor of N. (f) The E-FGR population transfer rates, corresponding to the solid lines in panels (a)–(e), as a function of the number of sites N, plotted on a log–log scale without the scale terms. The equilibrium rates are calculated with the collective approximation for $N = 10^3$ and 10^6 while without the collective approximation for $N = 5$ and 50.
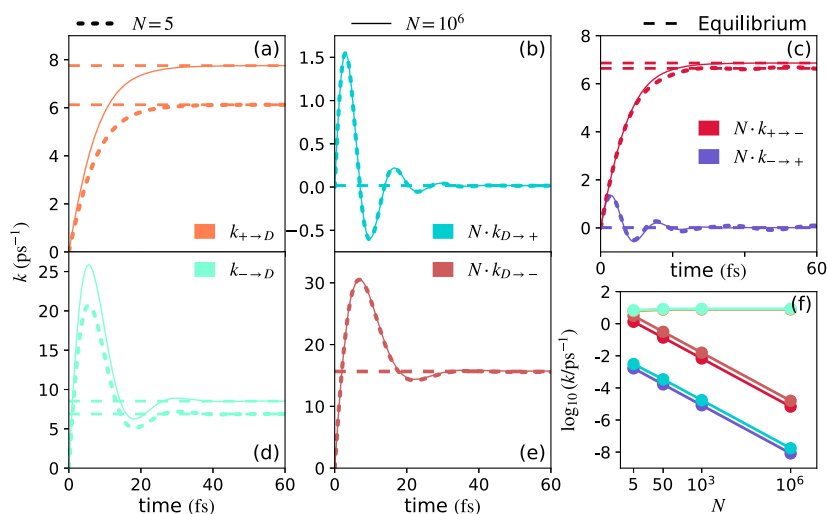

FIG. 3. The E-FGR and NE-FGR population transfer rates between the relevant states for a positive detuning $\Delta = 142$ meV, with the same quantities as shown in Fig. 2.

non-collective rates stay in a straight line with the collective rates means that the $C^0(t,s)$ term has a minor influence on the rate constants. The remaining two rates, $k_{\pm \to D}$, are expected to scale with $(N-1)/N$, which is close to a horizontal line on the log–log plot, which agrees with panel (f).

Another factor that affects the transition rates is the energy of the transition $\omega = \omega_i - \omega_f$. Ignoring the scaling involving N, all energetically favorable transitions have faster E-FGR rates than the energetically unfavorable transitions. On the other hand, the transient non-equilibrium rate can be many times larger than the corresponding E-FGR rates for energetically unfavorable $k_{- \to D}$, $k_{D \to +}$, and

$k_{- \to +}$. This is much less pronounced for the energetically favorable $k_{+ \to D}$, $k_{D \to -}$, and $k_{+ \to -}$.

Figure 3 presents the same plot as Fig. 2, with the positive detuning case, and Fig. 4 presents the rate constants with the negative detuning case. The change of detuning leads to two mutually antagonistic effects. For the positive detuning case, the model system has $+ \to \mathcal{D}$ transition energy that matches the peak of the function $J(\omega)[n(\omega) + 1]$ [see Fig. 1(b)] and $\mathcal{D} \to -$ farther away from resonance with $J(\omega)[n(\omega) + 1]$. This resonance between $\omega_+ - \omega_x$ and the peak value of $J(\omega)[n(\omega) + 1]$ is expected to promote the $+ \to \mathcal{D}$ transition rate and suppress the $\mathcal{D} \to -$ rate. On the other hand, the
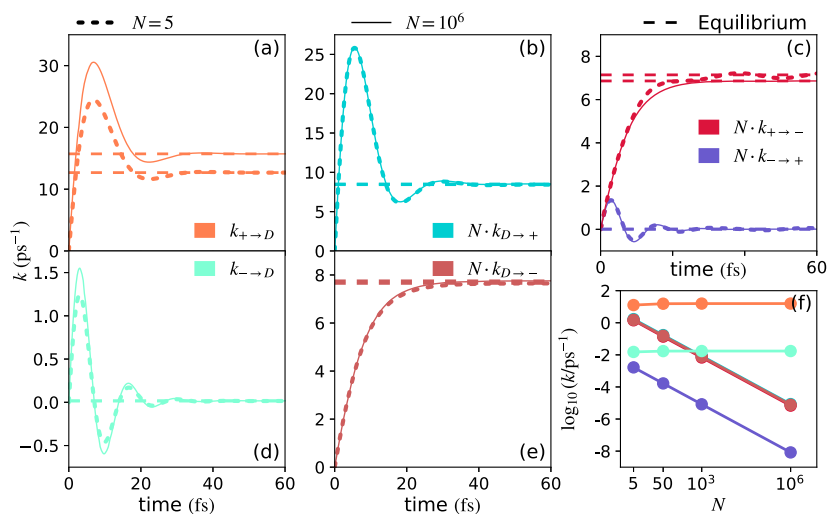

FIG. 4. The E-FGR and NE-FGR population transfer rates between the relevant states for a negative detuning case $\Delta = -142$ meV, with the same quantities as shown in Fig. 2.
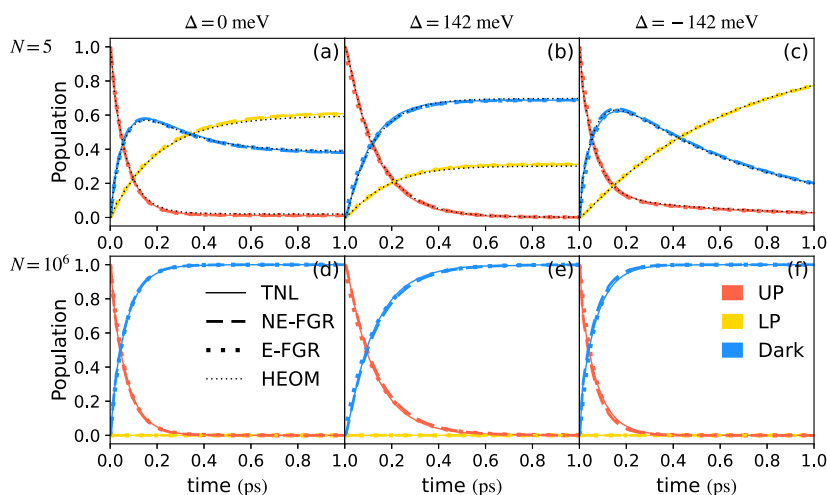

FIG. 5. Population dynamics with the initial state of $|+\rangle$, obtained using E-FGR [Eqs. (16b) and (27)], NE-FGR [Eqs. (16b) and (17)], and a quantum master equation-based time-nonlocal method [TNL, Eq. (11)], for $N = 5$ and the collective case of $N = 10^6$, with three different detunings. The population of the $|+\rangle$ state (red), the $|-\rangle$ state (orange), and the dark state manifold (blue) are presented. For a comparison with numerically exact results, the HEOM dynamics is also included for $N = 5$ as the thin black dashed lines.

positive detuning reduces the exciton component of the $|+\rangle$ state, which leads to a smaller $1 \pm \cos 2\phi$ pre-factor in Eq. (30a) and suppresses the $+ \to \mathcal{D}$ transition rate, while $\mathcal{D} \to -$ gets an increased pre-factor that promotes the transition rate. In the present case, the effect of the pre-factor turns out to be stronger than the resonance effect. Comparing Figs. 3(a) and 3(e) to Fig. 2, the positive detuning promotes $k_{D \to -}$ and suppresses $k_{+ \to D}$. Analogous observations can be made for negative detuning, Figs. 4(a) and 4(e), which promotes $k_{+ \to \mathcal{D}}$ and suppresses $k_{- \to \mathcal{D}}$ compared to the zero detuning case in Fig. 2.

For the energetically unfavorable rate constants $k_{D \to +}$ and $k_{- \to D}$, the effect of changing detuning is more straightforward. These rates are most sensitive to the transition energy $\omega_{\mathcal{K}\mathcal{J}}$ since they scale exponentially with $\beta \hbar \omega_{\mathcal{K}\mathcal{J}}$. As a result, $k_{- \to D}$ is promoted by the positive detuning, while $k_{D \to +}$ is promoted by the negative detuning.

We now consider the case where the upper polariton is initially populated, followed by population relaxation. Figure 5(a) presents the population dynamics for the $N = 5$ case with zero detuning $\Delta = 0$, where E-FGR (short dashed), NE-FGR (long dashed), and TNL (thin solid) are used to generate the population dynamics and are compared against the numerically exact solution from HEOM (dotted line). Figures 5(a) and 5(b) present the dynamics for $N = 5$, with the positive and negative detuning cases, respectively. Figures 5(d)–5(f) presents the corresponding dynamics, with $N = 10^6$, without the HEOM results. Among all of the approximate population dynamics, we consider the TNL [Eq. (11)] as the most accurate one because it only makes the second-order perturbation approximation of the system–bath coupling. The NE-FGR theory [Eq. (16a)] carries an additional approximation by using time local populations $P_k(t-s) \to P_k(t)$ compared to TNL QME. The E-FGR population dynamics [Eq. (27)] has the most approximations, which only uses the E-FGR rate in the population dynamics, compared to the NE-FGR population dynamics [Eq. (16b)]. For all of the

dynamics presented here, the three perturbative methods resulted in virtually identical dynamics. This means that the transient (~50 fs) difference between the three methods is not significant enough to influence the dynamics. The population dynamics therefore can be analyzed in the context of E-FGR, where in the case of $N = 5$, the lower polariton and dark states reach an equilibrium corresponding to the relative strength of $k_{D \to -}$ and $k_{- \to D}$. In the case of $N = 10^6$, the equilibrium populations consist of mostly dark states, consistent with predictions from the density of states argument and entropy-based analysis. Nevertheless, we must emphasize that for other model systems with different spectral densities $J(\omega)$, it is possible for NE-FGR and E-FGR to differ significantly, in which case NE-FGR is much preferable to use.

The accuracy of the NE-FGR and E-FGR dynamics is assessed by comparing them to the numerically exact hierarchical equations of motion (HEOM) method. Here, we only compute the exact population dynamics for $N = 5$ with HEOM. Figure 5 shows that E-FGR accurately captures the HEOM dynamics. This is expected since reorganization energy $\lambda = 14$ meV is chosen to be less than $k_B T \approx 26$ meV and $\sqrt{N}g_c = 50$ meV such that under this weak system–bath coupling condition, the perturbative approximation in FGR is valid. Furthermore, both NE-FGR and E-FGR are expected to be more accurate in the experimentally relevant collective regime because the off-diagonal system–bath coupling scales with $1/N$, making the perturbative approximation valid under the large N limit.

We now study a case where the effect of the transient difference between NE-FGR and E-FGR results in a more prominent difference in the dynamics. To this end, we consider the case where the lower polariton is initially populated, such that the short-time dynamics are dominated by energetically unfavorable $k_{- \to D}$ where the transient rate from NE-FGR is significantly larger than its equilibrium limit E-FGR rate. The resulting population dynamics are
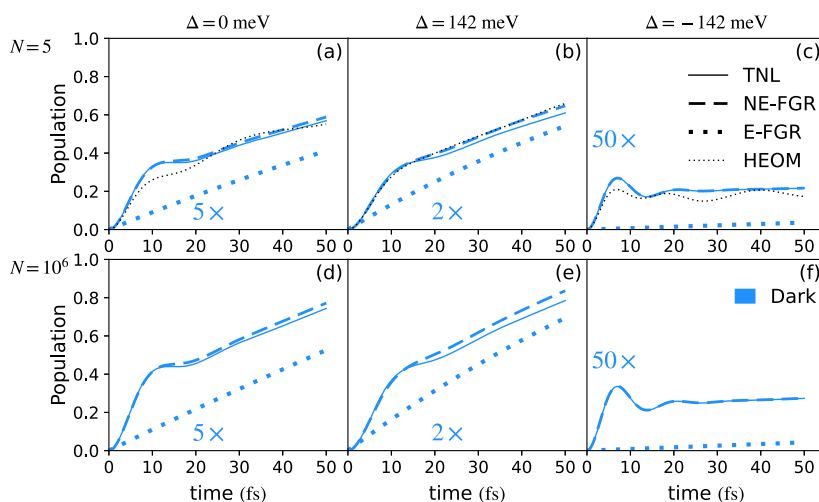

FIG. 6. Population dynamics with the initial state of $|-\rangle$, obtained from E-FGR [Eqs. (16b) and (27)], NE-FGR [Eqs. (16b) and (17)], and a quantum master equation-based time-nonlocal method [TNL, Eq. (11)] for the case of $N = 5$ [panels (a)–(c)] and the collective case of $N = 10^6$ [panels (d)–(f)] for various detunings. Here, we only plot the population of the dark state manifold (blue). To demonstrate the population dynamics more clearly, the $\mathcal{D}$ population is multiplied by different factors, as labeled in the corresponding panels. For a comparison with numerically exact results, the HEOM dynamics is also included for $N = 5$ as the thin black dashed plot lines.

showcased in Fig. 6. Since the upper polariton never receives any significant population ($P_+ \approx 0$), Fig. 6 only presents the dark state population for comparison (whereas the $P_- \approx 1 - P_{\mathcal{D}}$). Not surprisingly, the E-FGR underestimates the dark state population in all three cases of light–matter detunings since the E-FGR rate constant lacks the transient spike in $k_{-\to\mathcal{D}}(t)$ [see panel (d) in Figs. 2–4]. The deviation between NE-FGR and its time-nonlocal counterpart TNL is not significant since the relatively slow $|-\rangle \to |\mathcal{D}\rangle$ process makes $P_j(t) = P_j(t-s)$ a valid approximation [comparing Eq. (11) to Eq. (16a)]. Further comparing to the exact HEOM result reveals that the NE-FGR and TNL give very accurate dynamics. This means that NE-FGR captures some important non-Markovian nature of the dynamics. The E-FGR dynamics, on the other hand, has a substantial difference compared to the NE-FGR and HEOM dynamics, indicating that E-FGR and a simple rate equation are not adequate to capture the dynamics, and the full time-dependent NE-FGR rate expression is necessary for this case. This importance of using NE-FGR in the transient timescale is likely to be general for population dynamics starting from LP since in the collective regime, the dynamics would be dominated by $k_{-\to D}$, which does not scale unfavorably with $1/N$.

V. CONCLUSION

Rate theories, such as E-FGR, have been widely used in the studies of polaritonic relaxation processes. In the present paper, we derived the analytic expression of the non-equilibrium FGR expression for the polaritonic relaxation process. A rigorous, discretization-independent, and time-domain derivation is provided for E-FGR based on the quantum master equation (QME), where NE-FGR arises as a natural generalization to E-FGR. This formulation of NE-FGR yields transfer rates between polariton states and dark states. In particular, for the $|\pm\rangle \to |\mathcal{D}\rangle$ process, both the general formalism in Eq. (17) [with $C_{\pm\to\mathcal{D}}(t,s)$ in Eq. (23)] and the approximate expression $k_{\pm\to\mathcal{D}}(t)$ [Eq. (29)] are provided, which gives the analytic expression of the full time-dependent flux–side correlation function for the rate.

Under the collective limit ($N \gg 1$) and the Markovian limit ($t \to \infty$), the NE-FGR formalism reduces to the well-known E-FGR rate expression [frequency-domain formalism in Eq. (30a)]. Compared to the NE-FGR expressions, these E-FGR rate expressions have the same scaling relation in terms of N. The difference between the time-independent and time-dependent rate theory is tested via the application of E-FGR and NE-FGR to an experimentally relevant model system.[40,85] As expected, the time-dependent NE-FGR rates deviate from the E-FGR rate transiently before converging to the E-FGR rate constant on similar timescales for all six population transfers. The significance of this deviation is different for each population transfer process and is stronger for the energetically unfavorable population transitions. In the collective limit $N \to \infty$, the population dynamics is dominated by transfer from the polaritons to the dark states, which scales favorably with N. Therefore, the LP $\to \mathcal{D}$ rate shows the most significant deviation from the equilibrium rate in an experimentally relevant setting.

To further gauge the consequence of the time-dependent rate from NE-FGR theory, the E-FGR population dynamics are compared against that of NE-FGR as well as a time-nonlocal (TNL) master equation, which is a further generalization of NE-FGR. In our model system, given the relatively weak system–bath coupling $\lambda < k_B T$ chosen for the present trial, starting from the upper polariton yields coinciding dynamics for E-FGR, NE-FGR, and TNL. Hence, the non-Markovian effects are not significant for population dynamics starting from the $|+\rangle$ state for the current model system investigated in this work, but our NE-FGR formalism is general for the future investigation to explore any significant difference for other HTC model systems with different $J(\omega)$. Further comparing these dynamics to the numerically exact HEOM simulations for the case $N = 5$, we find that E-FGR, NE-FGR, and TNL all give very accurate dynamics in this weak system–bath coupling regime. Since the bath further decouples from the system [note the system–bath coupling $\propto c_a/\sqrt{N}$ in Eq. (A2)] under the collective limit ($N \to \infty$), TNL and NE-FGR are expected to be accurate in the experimentally relevant setting as well because the second order perturbation approximation is valid.

The non-Markovian characteristics of NE-FGR become more prominent for the population dynamics starting from the lower polariton. In this case, the dynamics are dominated by the $k_{-\to D}$ rate since the corresponding transfer starts from the lower polariton and the rate scales with N. Furthermore, $|-\rangle \to |\mathcal{D}\rangle$ being energetically unfavorable leads to a large difference between transient NE-FGR rates and the E-FGR rate, and the resulting NE-FGR population dynamics differ significantly from E-FGR in both non-collective and collective cases. A comparison to the numerical exact result shows a clear advantage of using NE-FGR over E-FGR to simulate the $|-\rangle \leftarrow \{|\mathcal{D}\rangle\}$ process. This advantage of NE-FGR is likely to exist for dynamics where the transient process is dominated by a transfer process from a polariton state to a higher-energy dark state. Future work will focus on incorporating static disorders in exciton energy, dipole orientation disorders, and cavity loss effects.

SUPPLEMENTARY MATERIAL

See the supplementary material for additional information on the derivation of the Hamiltonian in the polariton basis, the derivation of the FGR time correlation function, the derivation of the E-FGR expression in the frequency domain, and details of the exact quantum dynamics simulations.

ACKNOWLEDGMENTS

16 September 2024 13:37:38

AUTHOR DECLARATIONS

Author Contributions

Yifan Lai: Conceptualization (equal); Data curation (lead); Formal analysis (lead); Investigation (lead); Methodology (lead); Software (lead); Validation (lead); Visualization (lead); Writing – original draft (lead); Writing – review & editing (supporting). **Wenxiang Ying**: Conceptualization (equal); Data curation (equal); Formal analysis (equal); Investigation (equal); Methodology (equal); Software (equal); Validation (equal); Writing – original draft (supporting); Writing – review & editing (supporting). **Pengfei Huo**: Conceptualization (equal); Formal analysis (equal); Funding acquisition (lead); Investigation (equal); Project administration (lead); Supervision (lead); Visualization (equal); Writing – original draft (supporting); Writing – review & editing (lead).

DATA AVAILABILITY

The data that support the findings of this study are available from the corresponding author upon reasonable request.

APPENDIX A: EXPLICIT HAMILTONIAN EXPRESSION FOR RECIPROCAL SPACE AND POLARITONIC BASIS

Using the reciprocal space operators defined in Eqs. (4)–(6), the Hamiltonian in Eq. (1) is expressed as

$$
\begin{aligned}
\hat{H} = {} & \hbar\omega_x \sum_{j=0}^{N-1} \hat{D}_j^\dagger \hat{D}_j + \hbar\omega_c \hat{a}^\dagger \hat{a} + \sqrt{N}\hbar g\left(\hat{a}^\dagger \hat{B} + \hat{a}\hat{B}^\dagger\right) \\
& + \sum_{j=0}^{N-1} \sum_a \hbar\omega_a \hat{v}_{a,j}^\dagger \hat{v}_{a,j} \\
& + \left(\hat{B}^\dagger \hat{B} + \sum_{j=1}^{N-1} \hat{D}_j^\dagger \hat{D}_j\right) \otimes \sum_a \frac{c_a}{\sqrt{N}}\left(\hat{v}_{a,0}^\dagger + \hat{v}_{a,0}\right) \\
& + \sum_{j \neq k} \hat{D}_j^\dagger \hat{D}_k \sum_a \frac{c_a}{\sqrt{N}}\left(\hat{v}_{a,k-j}^\dagger + \hat{v}_{a,j-k}\right).
\end{aligned}
\tag{A1}
$$

Further diagonalizing the light–matter part of the Hamiltonian [Eq. (10)] and expressing the Hamiltonian in the polariton basis, we have

$$
\begin{aligned}
\hat{H} = {} & \hbar\omega_\pm \hat{P}_\pm^\dagger \hat{P}_\pm + \hbar\omega_x \sum_{j=1}^{N-1} \hat{D}_j^\dagger \hat{D}_j + \sum_{j=0}^{N-1} \sum_a \hbar\omega_a \hat{v}_{a,j}^\dagger \hat{v}_{a,j} + \left(\frac{1 + \cos 2\phi}{2}\hat{P}_+^\dagger \hat{P}_+ + \frac{1 - \cos 2\phi}{2}\hat{P}_-^\dagger \hat{P}_- + \sum_{j=1}^{N-1} \hat{D}_j^\dagger \hat{D}_j\right) \otimes \sum_a \frac{c_a}{\sqrt{N}}\left(\hat{v}_{a,0}^\dagger + \hat{v}_{a,0}\right) \\
& - \frac{\sin 2\phi}{2}\left(\hat{P}_+^\dagger \hat{P}_- + \hat{P}_+^\dagger \hat{P}_-\right) \otimes \sum_a \frac{c_a}{\sqrt{N}}\left(\hat{v}_{a,0}^\dagger + \hat{v}_{a,0}\right) + \sum_{j \neq k}^{N-1} \hat{D}_j^\dagger \hat{D}_k \otimes \sum_a \frac{c_a}{\sqrt{N}}\left(\hat{v}_{a,k-j}^\dagger + \hat{v}_{a,j-k}\right) + \cos\phi \sum_{j=1}^{N-1} \hat{P}_+^\dagger \hat{D}_j \otimes \sum_a \frac{c_a}{\sqrt{N}}\left(\hat{v}_{a,j}^\dagger + \hat{v}_{a,-j}\right) \\
& - \sin\phi \sum_{j=1}^{N-1} \hat{P}_-^\dagger \hat{D}_j \otimes \sum_a \frac{c_a}{\sqrt{N}}\left(\hat{v}_{a,j}^\dagger + \hat{v}_{a,-j}\right) + h.c.
\end{aligned}
\tag{A2}
$$

which serves as the working Hamiltonian for the derivation of all FGR expressions. The reader can refer to Sec. I of the supplementary material for a detailed derivation of the delocalized and polaritonic Hamiltonian.

APPENDIX B: EVALUATION OF BATH CORRELATION FUNCTIONS

In this work, a Brownian form of the single-site bath spectral density is used, which has the following expression:

$$
J(\omega) = \frac{4\lambda\eta\omega\Omega^2}{\left(\omega^2 - \Omega^2\right)^2 + 4\eta^2\omega^2},
\tag{B1}
$$

where the oscillator is underdamped, $\eta < \Omega$. In this case, the high-temperature friction kernel can be evaluated analytically as follows:

$$
\gamma(t) = \gamma_{\beta=0}(t) = \lambda e^{-\eta t}\left(\frac{\eta}{\xi}\sin\xi t + \cos\xi t\right)
$$

$$
\dot{\gamma}(t) = \dot{\gamma}_{\beta=0}(t) = -\frac{\lambda\Omega^2}{\xi}e^{-\eta t}\sin\xi t
$$

$$
\begin{aligned}
\Gamma(t) = {} & \Gamma_{\beta=0}(t) \\
= {} & \frac{\lambda}{\Omega^2}\left(2e^{-\frac{1}{2}\eta t}\eta^2 t\operatorname{sinhc}\frac{1}{2}\eta t + e^{-\eta t}\eta\xi^2 t^2\operatorname{sinc}^2\frac{1}{2}\xi t \right. \\
& \left. + e^{-\eta t}(\xi^2 - \eta^2)t\operatorname{sinc}\xi t\right),
\end{aligned}
\tag{B2}
$$

where $\xi = \sqrt{\Omega^2 - \eta^2}$. The cardinal hyperbolic sine function is defined as $\operatorname{sinhc} x = \sinh x/x = \operatorname{sinc} ix$. Note that Eq. (B2) is only true for the specific form of $J(\omega)$, which is Brownian.

The finite-temperature friction kernel γ_β and its antiderivatives $\Gamma_\beta, \bar{\Gamma}_\beta$ have to be evaluated numerically and could cause a numerical challenge because of the oscillatory behaving integrand inside the integrals in Eqs. (22) and (25). Instead, γ_β can be evaluated using the

following integration over a non-oscillatory function:

$$\gamma_\beta(t) = -\frac{1}{2}\int_0^\infty d\tau \, \coth\frac{\pi\tau}{\beta\hbar} \, [\dot\gamma(\tau - t) + \dot\gamma(\tau + t)], \qquad (B3)$$

where $\dot\gamma$ is an odd function and can be evaluated analytically using Eq. (B2). The validity of the above identity in Eq. (B3) can be easily verified by using the definition of $\dot\gamma$ in Eq. (22) and the Fourier transform of the hyperbolic cotangent,

$$\int_0^\infty d\tau \, \coth\tau \, \sin\omega\tau = \coth\frac{\pi}{2}\omega. \qquad (B4)$$

Furthermore, Eq. (B3) leads to similar expressions for $\Gamma_\beta, \bar\Gamma_\beta$,

$$\Gamma_\beta(t) = \frac{1}{2}\int_0^\infty d\tau \, \coth\frac{\pi\tau}{\beta\hbar} \, [\gamma(\tau - t) - \gamma(\tau + t)]$$

$$\bar\Gamma_\beta(t) = \int_0^\infty d\tau \, \coth\frac{\pi\tau}{\beta\hbar} \, [2\Gamma(\tau) - \Gamma(\tau - t) - \Gamma(\tau + t)], \qquad (B5)$$

where γ (Γ) are even (odd) functions. In the present application, the time integrals Eqs. (B3) and (B5) are evaluated numerically using the standard integration package in Scipy.

APPENDIX C: EVALUATION OF COLLECTIVE E-FGR RATES

After eliminating the $C^0_{\mathcal{J}\to K}$ term in the collective limit and extending the integration limit to infinity under the equilibrium approximation, the evaluation of rate constants Eq. (16b) is reduced to Fourier transforming $C_{D\to D}(s)$, which can be evaluated analytically as

$$\frac{1}{\hbar^2}\int_{-\infty}^\infty ds \, C_{D\to D}(s)e^{-i\omega s}$$

$$= \frac{1}{\hbar^2}\int_{-\infty}^\infty ds \sum_a \frac{c_a^2}{N}\left[\frac{e^{i(\omega_a - \omega)s}}{e^{\beta\hbar\omega_a} - 1} + \frac{e^{-i(\omega_a + \omega)s}}{1 - e^{-\beta\hbar\omega_a}}\right]$$

$$= \frac{2\pi}{\hbar^2}\sum_a \frac{c_a^2}{N}\left[\frac{\delta(\omega_a - \omega)}{e^{\beta\hbar\omega_a} - 1} + \frac{\delta(\omega_a + \omega)}{1 - e^{-\beta\hbar\omega_a}}\right]$$

$$= \frac{2\pi}{N\hbar^2}\left[\frac{\sum_a c_a^2\delta(\omega_a - \omega)}{e^{\beta\hbar\omega} - 1} + \frac{\sum_a c_a^2\delta(\omega_a + \omega)}{1 - e^{\beta\hbar\omega}}\right]$$

$$= \frac{2}{N\hbar}\left[\frac{J(\omega)}{e^{\beta\hbar\omega} - 1} + \frac{J(-\omega)}{1 - e^{\beta\hbar\omega}}\right] = \frac{2}{N\hbar}\frac{J(|\omega|)}{|e^{\beta\hbar\omega} - 1|}, \qquad (C1)$$

which upon including the appropriate prefactors yields the collective E-FGR rate constants in Eq. (30a).

The E-FGR rate constant can also be obtained from the $t \to \infty$ limit of Eq. (29). Here, we utilize the identity $\lim_{t\to\infty}\sin(\omega t)/\pi\omega = \delta(\omega)$, yielding

$$k_{\pm\to\mathcal{D}}(t \to \infty) = \frac{N-1}{2N\hbar}(1 \pm \cos 2\phi)\int_0^\infty d\omega J(\omega)\coth\left(\frac{1}{2}\beta\hbar\omega\right)$$

$$\times (\delta(\omega + \omega_\pm - \omega_x) + \delta(\omega - \omega_\pm + \omega_x))$$

$$+ \frac{N-1}{2N\hbar}(1 \pm \cos 2\phi)\int_0^\infty d\omega J(\omega)$$

$$\times (\delta(\omega + \omega_\pm - \omega_x) - \delta(\omega - \omega_\pm + \omega_x)), \qquad (C2)$$

which is equivalent to Eq. (30a).

REFERENCES

[1] A. Mandal, M. A. Taylor, B. M. Weight, E. R. Koessler, X. Li, and P. Huo, "Theoretical advances in polariton chemistry and molecular cavity quantum electrodynamics," Chem. Rev. **123**, 9786–9879 (2023).

[2] A. Kavokin and G. Malpuech, *Cavity Polaritons* (Elsevier, San Diego, 2003).

[3] W. Ahn, J. F. Triana, F. Recabal, F. Herrera, and B. S. Simpkins, "Modification of ground-state chemical reactivity via light–matter coherence in infrared cavities," Science **380**, 1165–1168 (2023).

[4] H. Zeng, J. B. Pérez-Sánchez, C. T. Eckdahl, P. Liu, W. J. Chang, E. A. Weiss, J. A. Kalow, J. Yuen-Zhou, and N. P. Stern, "Control of photoswitching kinetics with strong light–matter coupling in a cavity," J. Am. Chem. Soc. **145**, 19655–19661 (2023).

[5] A. Sau, K. Nagarajan, B. Patrahau, L. Lethuillier-Karl, R. M. A. Vergauwe, A. Thomas, J. Moran, C. Genet, and T. W. Ebbesen, "Modifying Woodward–Hoffmann stereoselectivity under vibrational strong coupling," Angew. Chem., Int. Ed., **60**, 5712–5717 (2021).

[6] K. Nagarajan, A. Thomas, and T. W. Ebbesen, "Chemistry under vibrational strong coupling," J. Am. Chem. Soc., **143**, 16877–16889 (2021).

[7] A. Mandal and P. Huo, "Investigating new reactivities enabled by polariton photochemistry," J. Phys. Chem. Lett., **10**, 5519–5529 (2019).

[8] J. Feist, J. Galego, and F. J. Garcia-Vidal, "Polaritonic chemistry with organic molecules," ACS Photonics **5**, 205–216 (2018).

[9] K. Stranius, M. Hertzog, and K. Börjesson, "Selective manipulation of electronically excited states through strong light–matter interactions," Nat. Commun. **9**, 2273 (2018).

[10] B. Munkhbat, M. Wersäll, D. G. Baranov, T. J. Antosiewicz, and T. Shegai, "Suppression of photo-oxidation of organic chromophores by strong coupling to plasmonic nanoantennas," Sci. Adv. **4**, eaas9552 (2018).

[11] R. F. Ribeiro, L. A. Martínez-Martínez, M. Du, J. Campos-Gonzalez-Angulo, and J. Yuen-Zhou, "Polariton chemistry: Controlling molecular dynamics with optical cavities," Chem. Sci. **9**, 6325–6339 (2018).

[12] A. Canaguier-Durand, C. Genet, A. Lambrecht, T. W. Ebbesen, and S. Reynaud, "Non-Markovian polariton dynamics in organic strong coupling," Eur. Phys. J. D **69**, 24 (2015).

[13] W. Ying and P. Huo, "Resonance theory and quantum dynamics simulations of vibrational polariton chemistry," J. Chem. Phys. **159**, 084104 (2023).

[14] W. Ying, M. A. D. Taylor, and P. Huo, "Resonance theory of vibrational polariton chemistry at the normal incidence," Nanophotonics **13**, 2601–2615 (2024).

[15] D. Hu, W. Ying, and P. Huo, "Resonance enhancement of vibrational polariton chemistry obtained from the mixed quantum-classical dynamics simulations," J. Phys. Chem. Lett., **14**, 11208–11216 (2023).

[16] W. Ying and P. Huo, "Resonance theory of vibrational strong coupling enhanced polariton chemistry and the role of photonic mode lifetime," Commun. Mater. **5**, 110 (2024).

[17] S. Montillo Vega, W. Ying, and P. Huo, "Theory of resonance suppression in vibrational polariton chemistry," chemRxiv:2024-m7t4c (2024).

[18] D. Xu, A. Mandal, J. M. Baxter, S.-W. Cheng, I. Lee, H. Su, S. Liu, D. R. Reichman, and M. Delor, "Ultrafast imaging of polariton propagation and interactions," Nat. Commun. **14**, 3881 (2023).

[19] R. H. Tichauer, I. Sokolovskii, and G. Groenhof, "Tuning the coherent propagation of organic exciton-polaritons through the cavity Q-factor," Adv. Sci. **10**, 2302650 (2023).

[20] I. Sokolovskii, R. H. Tichauer, D. Morozov, J. Feist, and G. Groenhof, "Multiscale molecular dynamics simulations of enhanced energy transfer in organic molecules under strong coupling," Nat. Commun. **14**, 6613 (2023).

[21] R. Pandya, A. Ashoka, K. Georgiou, J. Sung, R. Jayaprakash, S. Renken, L. Gai, Z. Shen, A. Rao, and A. J. Musser, "Tuning the coherent propagation of organic exciton-polaritons through dark state delocalization," Adv. Sci. **9**, 2105569 (2022).

[22] R. Pandya, R. Y. S. Chen, Q. Gu, J. Sung, C. Schnedermann, O. S. Ojambati, R. Chikkaraddy, J. Gorman, G. Jacucci, O. D. Onelli, T. Willhammar, D. N. Johnstone, S. M. Collins, P. A. Midgley, F. Auras, T. Baikie, R. Jayaprakash, F. Mathevet, R. Soucek, M. Du, A. M. Alvertis, A. Ashoka, S. Vignolini, D. G. Lidzey, J. J. Baumberg, R. H. Friend, T. Barisien, L. Legrand, A. W. Chin, J. Yuen-Zhou, S. K. Saikin, P. Kukura, A. J. Musser, and A. Rao, "Microcavity-like exciton-polaritons can be

the primary photoexcitation in bare organic semiconductors," Nat. Commun. **12**, 6519 (2021).

[23] Y. Zakharko, M. Rother, A. Graf, B. Hähnlein, M. Brohmann, J. Pezoldt, and J. Zaumseil, "Radiative pumping and propagation of plexitons in diffractive plasmonic crystals," Nano Lett. **18**, 4927–4933 (2018).

[24] G. G. Rozenman, K. Akulov, A. Golombek, and T. Schwartz, "Long-range transport of organic exciton-polaritons revealed by ultrafast microscopy," ACS Photonics **5**, 105–110 (2018).

[25] G. Lerario, A. Fieramosca, F. Barachati, D. Ballarini, K. S. Daskalakis, L. Dominici, M. De Giorgi, S. A. Maier, G. Gigli, S. Kéna-Cohen, and D. Sanvitto, "Room-temperature superfluidity in a polariton condensate," Nat. Phys. **13**, 837–841 (2017).

[26] A. Gianfrate, L. Dominici, O. Voronych, M. Matuszewski, M. Stobińska, D. Ballarini, M. De Giorgi, G. Gigli, and D. Sanvitto, "Superluminal X-waves in a polariton quantum fluid," Light: Sci. Appl. **7**, 17119 (2017).

[27] M. Sich, D. N. Krizhanovskii, M. S. Skolnick, A. V. Gorbach, R. Hartley, D. V. Skryabin, E. A. Cerda-Méndez, K. Biermann, R. Hey, and P. V. Santos, "Observation of bright polariton solitons in a semiconductor microcavity," Nat. Photonics **6**, 50–55 (2012).

[28] T. Freixanet, B. Sermage, A. Tiberj, and R. Planel, "In-plane propagation of excitonic cavity polaritons," Phys. Rev. B **61**, 7233–7236 (2000).

[29] J. del Pino, J. Feist, and F. J. Garcia-Vidal, "Quantum theory of collective strong coupling of molecular vibrations with a microcavity mode," New J. Phys. **17**, 053040 (2015).

[30] T. Neuman and J. Aizpurua, "Origin of the asymmetric light emission from molecular exciton–polaritons," Optica **5**, 1247 (2018).

[31] T. E. Li, A. Nitzan, and J. E. Subotnik, "Polariton relaxation under vibrational strong coupling: Comparing cavity molecular dynamics simulations against Fermi's golden rule rate," J. Chem. Phys. **156**, 134106 (2022).

[32] J. B. Pérez-Sánchez, A. Koner, N. P. Stern, and J. Yuen-Zhou, "Simulating molecular polaritons in the collective regime using few-molecule models," Proc. Natl. Acad. Sci. U. S. A. **120**, e2219223120 (2023).

[33] F. Herrera and F. C. Spano, "Theory of nanoscale organic cavities: The essential role of vibration-photon dressed states," ACS Photonics **5**, 65–79 (2018).

[34] F. Herrera and F. C. Spano, "Cavity-controlled chemistry in molecular ensembles," Phys. Rev. Lett. **116**, 238301 (2016).

[35] S. Takahashi and K. Watanabe, "Decoupling from a thermal bath via molecular polariton formation," J. Phys. Chem. Lett. **11**, 1349–1356 (2020).

[36] M. E. Mondal, E. R. Koessler, J. Provazza, A. N. Vamivakas, S. T. Cundiff, T. D. Krauss, and P. Huo, "Quantum dynamics simulations of the 2D spectroscopy for exciton polaritons," J. Chem. Phys. **159**, 094102 (2023).

[37] A. G. Avramenko and A. S. Rury, "Quantum control of ultrafast internal conversion using nanoconfined virtual photons," J. Phys. Chem. Lett. **11**, 1013–1021 (2020).

[38] K. Peng and E. Rabani, "Polaritonic bottleneck in colloidal quantum dots," Nano Lett. **23**, 10587–10593 (2023).

[39] M. Laitz, A. E. K. Kaplan, J. Deschamps, U. Barotov, A. H. Proppe, I. García-Benito, A. Osherov, G. Grancini, D. W. deQuilettes, K. A. Nelson, M. G. Bawendi, and V. Bulović, "Uncovering temperature-dependent exciton-polariton relaxation mechanisms in hybrid organic-inorganic perovskites," Nat. Commun. **14**, 2426 (2023).

[40] L. Qiu, A. Mandal, O. Morshed, M. T. Meidenbauer, W. Girten, P. Huo, A. N. Vamivakas, and T. D. Krauss, "Molecular polaritons generated from strong coupling between CdSe nanoplatelets and a dielectric optical cavity," J. Phys. Chem. Lett. **12**, 5030–5038 (2021).

[41] B. Xiang, R. F. Ribeiro, L. Chen, J. Wang, M. Du, J. Yuen-Zhou, and W. Xiong, "State-selective polariton to dark state relaxation dynamics," J. Phys. Chem. A **123**, 5918–5927 (2019).

[42] J. Mony, M. Hertzog, K. Kushwaha, and K. Börjesson, "Angle-independent polariton emission lifetime shown by perylene hybridized to the vacuum field inside a Fabry–Pérot cavity," J. Phys. Chem. C **122**, 24917–24923 (2018).

[43] T. Schwartz, J. A. Hutchison, J. Léonard, C. Genet, S. Haacke, and T. W. Ebbesen, "Polariton dynamics under strong light–molecule coupling," ChemPhysChem **14**, 125–131 (2013).

[44] H.-D. Meyer, U. Manthe, and L. Cederbaum, "The multi-configurational time-dependent Hartree approach," Chem. Phys. Lett. **165**, 73–78 (1990).

[45] U. Manthe, H. Meyer, and L. S. Cederbaum, "Wave-packet dynamics within the multiconfiguration Hartree framework: General aspects and application to NOCl," J. Chem. Phys. **97**, 3199–3213 (1992).

[46] M. Beck, A. Jäckle, G. Worth, and H.-D. Meyer, "The multiconfiguration time-dependent Hartree (MCTDH) method: A highly efficient algorithm for propagating wavepackets," Phys. Rep. **324**, 1–105 (2000).

[47] H. Wang and M. Thoss, "Multilayer formulation of the multiconfiguration time-dependent Hartree theory," J. Chem. Phys. **119**, 1289–1299 (2003).

[48] H. Wang, "Multilayer multiconfiguration time-dependent Hartree theory," J. Phys. Chem. A **119**, 7951–7965 (2015).

[49] Y. Tanimura, "Nonperturbative expansion method for a quantum system coupled to a harmonic-oscillator bath," Phys. Rev. A **41**, 6676–6687 (1990).

[50] Y. Tanimura, "Stochastic Liouville, Langevin, Fokker–Planck, and master equation approaches to quantum dissipative systems," J. Phys. Soc. Jpn. **75**, 082001 (2006).

[51] R.-X. Xu, P. Cui, X.-Q. Li, Y. Mo, and Y. Yan, "Exact quantum master equation via the calculus on path integrals," J. Chem. Phys. **122**, 041103 (2005).

[52] R.-X. Xu and Y. Yan, "Dynamics of quantum dissipation systems interacting with bosonic canonical bath: Hierarchical equations of motion approach," Phys. Rev. E **75**, 031107 (2007).

[53] D. Hu, A. Mandal, B. M. Weight, and P. Huo, "Quasi-diabatic propagation scheme for simulating polariton chemistry," J. Chem. Phys. **157**, 194109 (2022).

[54] W. Zhou, D. Hu, A. Mandal, and P. Huo, "Nuclear gradient expressions for molecular cavity quantum electrodynamics simulations using mixed quantum-classical methods," J. Chem. Phys. **157**, 104118 (2022).

[55] R. H. Tichauer, J. Feist, and G. Groenhof, "Multi-scale dynamics simulations of molecular polaritons: The effect of multiple cavity modes on polariton relaxation," J. Chem. Phys. **154**, 104112 (2021).

[56] Y. Lai and E. Geva, "On simulating the dynamics of electronic populations and coherences via quantum master equations based on treating off-diagonal electronic coupling terms as a small perturbation," J. Chem. Phys. **155**, 204101 (2021).

[57] X. Sun and E. Geva, "Non-Condon equilibrium Fermi's golden rule electronic transition rate constants via the linearized semiclassical method," J. Chem. Phys. **144**, 244105 (2016).

[58] E. Suyabatmaz and R. F. Ribeiro, "Vibrational polariton transport in disordered media," J. Chem. Phys. **159**, 034701 (2023).

[59] D. Jasrasaria and E. Rabani, "Circumventing the phonon bottleneck by multiphonon-mediated hot exciton cooling at the nanoscale," npj Comput. Mater. **9**, 145 (2023).

[60] L. Mauro, K. Caicedo, G. Jonusauskas, and R. Avriller, "Charge-transfer chemical reactions in nanofluidic Fabry-Pérot cavities," Phys. Rev. B **103**, 165412 (2021).

[61] P. Michetti and G. C. La Rocca, "Simulation of J-aggregate microcavity photoluminescence," Phys. Rev. B **77**, 195301 (2008).

[62] X. Sun and E. Geva, "Non-Condon nonequilibrium Fermi's golden rule rates from the linearized semiclassical method," J. Chem. Phys. **145**, 064109 (2016).

[63] X. Sun, X. Zhang, and Z. Liu, "Generalized nonequilibrium Fermi's golden rule and its semiclassical approximations for electronic transitions between multiple states," J. Chem. Phys. **160**, 034108 (2024).

[64] X. Sun and Z. Liu, "Semiclassical approaches to perturbative time-convolution and time-convolutionless quantum master equations for electronic transitions in multistate systems," J. Chem. Phys. **160**, 174113 (2024).

[65] A. Montoya-Castillo, T. C. Berkelbach, and D. R. Reichman, "Extending the applicability of Redfield theories into highly non-Markovian regimes," J. Chem. Phys. **143**, 194108 (2015).

[66] J. H. Fetherolf and T. C. Berkelbach, "Linear and nonlinear spectroscopy from quantum master equations," J. Chem. Phys. **147**, 244109 (2017).

[67] C. W. Kim and I. Franco, "General framework for quantifying dissipation pathways in open quantum systems. II. Numerical validation and the role of non-Markovianity," J. Chem. Phys. **160**, 214112 (2024).

[68] F. Herrera and F. C. Spano, "Dark vibronic polaritons and the spectroscopy of organic microcavities," Phys. Rev. Lett. **118**, 223601 (2017).

[69] A. Caldeira and A. Leggett, "Quantum tunnelling in a dissipative system," Ann. Phys. **149**, 374–456 (1983).

[70] M. Tavis and F. W. Cummings, "Approximate solutions for an *N*-molecule-radiation-field Hamiltonian," Phys. Rev. **188**, 692–695 (1969).

[71] B. X. K. Chng, W. Ying, Y. Lai, A. N. Vamivakas, S. T. Cundiff, T. D. Krauss, and P. Huo, "Mechanism of polariton decoherence in the collective light-matter couplings regime," chemRxiv-2024-w70hr (2024).

[72] J. A. Campos-Gonzalez-Angulo and J. Yuen-Zhou, "Generalization of the Tavis–Cummings model for multi-level anharmonic systems: Insights on the second excitation manifold," J. Chem. Phys. **156**, 194308 (2022).

[73] H.-P. Breuer and F. Petruccione, *The Theory of Open Quantum Systems* (Clarendon, Oxford, 2007).

[74] P. Huo, T. F. Miller III, and D. F. Coker, "Communication: Predictive partial linearized path integral simulation of condensed phase electron transfer dynamics," J. Chem. Phys. **139**, 151103 (2013).

[75] D. Chandler, "Statistical mechanics of isomerization dynamics in liquids and the transition state approximation," J. Chem. Phys. **68**, 2959–2970 (1978).

[76] W. H. Miller, "Quantum mechanical transition state theory and a new semiclassical model for reaction rate constants," J. Chem. Phys. **61**, 1823–1834 (1974).

[77] U. Weiss, *Quantum Dissipative Systems*, 4th ed. (World Scientific Publishing Company, Singapore, 2012).

[78] G. D. Scholes, C. A. DelPo, and B. Kudisch, "Entropy reorders polariton states," J. Phys. Chem. Lett. **11**, 6389–6395 (2020).

[79] T. Gera and K. L. Sebastian, "Exact results for the Tavis-Cummings and Hückel Hamiltonians with diagonal disorder," J. Phys. Chem. A **126**, 5449–5457 (2022).

[80] G. Engelhardt and J. Cao, "Unusual dynamical properties of disordered polaritons in microcavities," Phys. Rev. B **105**, 064205 (2022).

[81] K. Schwennicke, N. C. Giebink, and J. Yuen-Zhou, "Extracting accurate light–matter couplings from disordered polaritons," Nanophotonics **13**, 2469–2478 (2024).

[82] Z. Zhou, H.-T. Chen, J. E. Subotnik, and A. Nitzan, "Interplay between disorder, local relaxation, and collective behavior for an ensemble of emitters outside versus inside a cavity," Phys. Rev. A **108**, 023708 (2023).

[83] J. B. Pérez-Sánchez, F. Mellini, N. C. Giebink, and J. Yuen-Zhou, "Collective polaritonic effects on chemical dynamics suppressed by disorder," Phys. Rev. Res. **6**, 013222 (2024).

[84] R. Houdré, R. P. Stanley, and M. Ilegems, "Vacuum-field Rabi splitting in the presence of inhomogeneous broadening: Resolution of a homogeneous linewidth in an inhomogeneously broadened system," Phys. Rev. A **53**, 2711–2715 (1996).

[85] M. Amin, E. R. Koessler, O. Morshed, F. Awan, N. M. B. Cogan, R. Collison, T. Tumiel, W. Girten, C. S. Leiter, A. N. Vamivakas, P. Huo, and T. D. Krauss, "Cavity controlled upconversion in CdSe nanoplatelet polaritons," ACS Nano **18**, 21388–21398 (2024).

[86] T. Ozaki, "Continued fraction representation of the Fermi-Dirac function for large-scale electronic structure calculations," Phys. Rev. B **75**, 035123 (2007).

[87] J. Hu, R.-X. Xu, and Y. Yan, "Communication: Padé spectrum decomposition of Fermi function and Bose function," J. Chem. Phys. **133**, 101106 (2010).

[88] J. Hu, M. Luo, F. Jiang, R.-X. Xu, and Y. Yan, "Padé spectrum decompositions of quantum distribution functions and optimal hierarchical equations of motion construction for quantum open systems," J. Chem. Phys. **134**, 244106 (2011).

16 September 2024 13:37:38